ISSN: 26614952

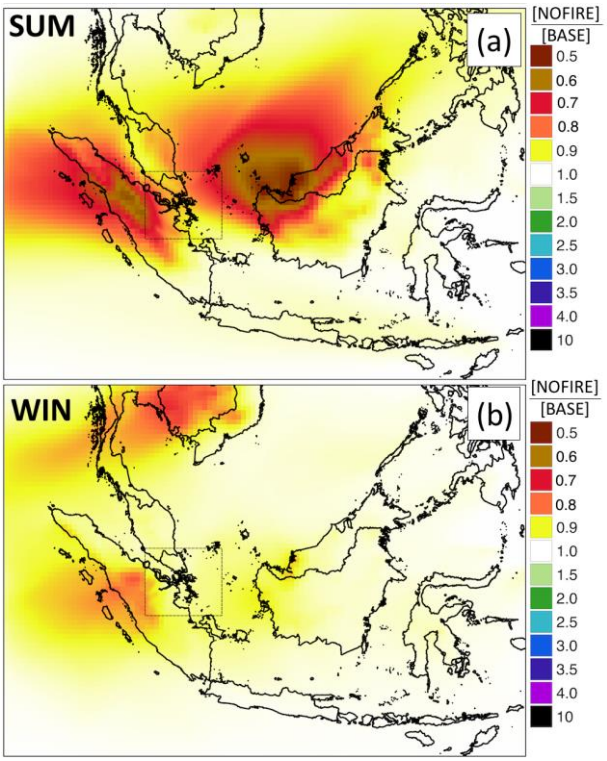

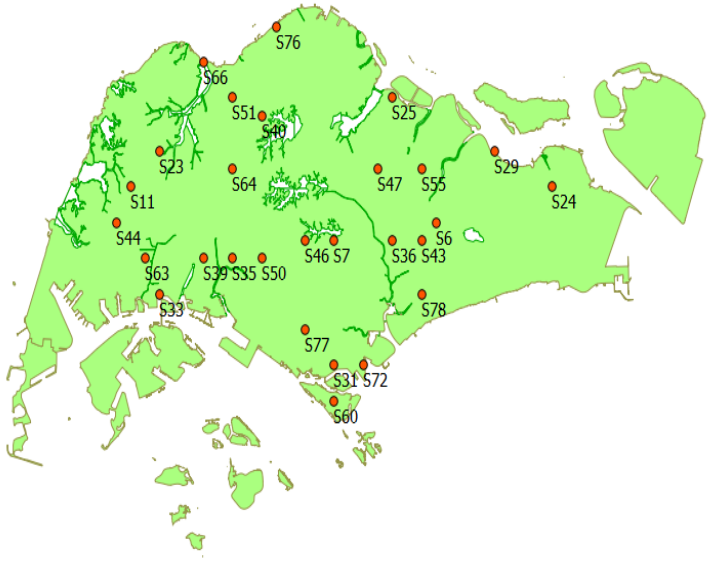

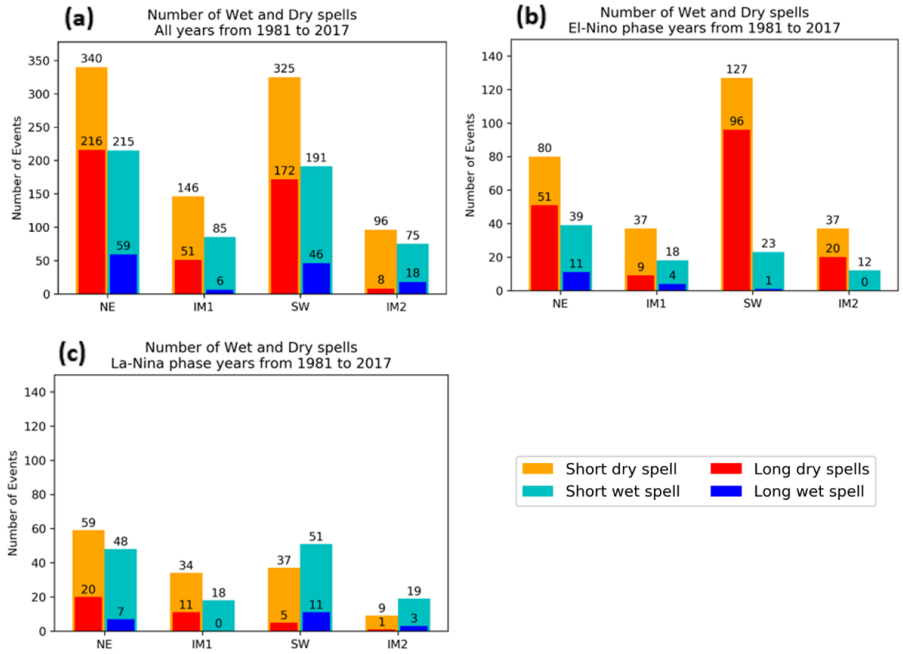

MSS RESEARCH LETTERS

Issue #6, March 2021

METEOROLOGICAL SERVICE SINGAPORE

ISSN: 26614952

DISCLAIMER OF WARRANTIES AND LIABILITY

1. While National Environment Agency Meteorological Service Singapore (NEA MSS) has made every reasonable effort to ensure that the information contained in this publication has been obtained from reliable sources, NEA MSS shall not be responsible for any errors or omissions, or for the results obtained from the use of such information.

2. NEA MSS shall also not be liable for any damage or loss of any kind howsoever caused as a result of any reliance on the contents of this publication.

EDITOR'S NOTE.

Dear Readers,

I am happy to present the sixth issue of MSS Research Letters. I also take this opportunity to wish all our readers a very happy 2021! The year 2020 was an unpredictable ride through the pandemic, with many challenges for people across the globe. Let's embrace 2021 with a positive and cheery spirit that will help us cope with this current situation until we see light at the end of the tunnel.

The sixth issue of MSS research Letters presents three articles. All three have been contributed by our MSS staff. The first letter is an interesting case study on 2008-2009 seasonal pollution plumes over Singapore showing that they vary with respect to monsoon season with their impact being severe during the winter monsoon. The second letter involves a locally-tuned Heavy Rain Total Threat Score tool that can be used as an early indicator of heavy rain events hours before flash flood occurrences in Singapore. The third and final letter is on the characterisation of wet and dry spells within monsoon seasons over the Malaysian peninsula and Singapore.

I would like to thank the authors and reviewers of this issue, for their valuable contributions. My sincere acknowledgement goes to Micheline Fong who has helped through the various stages of the editorial tasks of the MSS Research Letters.

Enjoy this issue of MSS Research Letters, and I am looking forward to having more contributions in the next issues. ☺

Take care and stay safe,
Hindumathi Palanisamy
Editor, MSS Research Letters

Cover figures: top left – Seasonal mean concentrations of O_3, in [NOFIRE] as a relative fraction of [BASE], during the (a) summer monsoon and (b) winter monsoon. The sub-regional simulation is overlaid on the regional simulation (Page 8); top right – Map of Singapore showing the locations of the 28 rainfall stations used for climate monitoring (bottom right alpha-numbers indicate the station codes) (Page 14); bottom – Number of wet and dry spells from 1981 to 2017 calculated using CHIRPS, for (a) all years, (b) El-Niño phase years only, (c) La-Niña phase years only computed for the domain of interest (Page 29).

TABLE OF CONTENTS

Seasonal Pollution Plumes over Singapore: April 2008 - March 2009 Case study

Sean Lee[1,2], Sebastian D. Eastham[3], Akshay Ashok[1, 3], Xian-Xiang Li[1, 4], Florian Allroggen[3], Steve H.L. Yim[1, 5], Steven R.H. Barrett[1, 3], Leslie K. Norford[1, 6]

[1] *Center for Environmental Sensing and Modelling, Singapore-MIT Alliance for Research and Technology*
[2] *Department of Weather Research, Centre for Climate Research Singapore*
[3] *Department of Aeronautics and Astronautics, Massachusetts Institute of Technology*
[4] *School of Atmospheric Sciences, Sun Yat-Sen University*
[5] *Department of Geography and Resource Management, The Chinese University of Hong Kong*
[6] *Department of Architecture, Massachusetts Institute of Technology*

ABSTRACT

A 1.4 km-resolution simulation of air quality over Singapore using the Community Multiscale Air Quality (CMAQ) model was verified against measurements from 14 monitoring sites on the island, for the period of April 2008 to March 2009. Ozone and nitrogen dioxide were generally well-simulated, but less so when they fell under pollution plumes downstream of power stations. The plumes vary with monsoon season and their impact on domestic air quality was more severe during the winter monsoon.

1 INTRODUCTION

Poor air quality has been shown to impact human health. Long-term exposure to ambient ozone (O_3) and fine particulate matter ($PM_{2.5}$) has been repeatedly linked with increased risk of premature mortality and morbidity (Burnett et al., 2014; Hoek et al., 2013), and the World Health Organization (WHO) has indicated that exposure to other air pollutants such as nitrogen dioxide and sulphur dioxide may constitute a health risk (WHO, 2013, 2016a, 2016b). The annual cost of the health impact due to air pollution for the East Asia and Pacific region was estimated to be 4.5% of the regional Gross Domestic Product (The World Bank, 2016). The Singapore government sought to meet the 2005-revision of WHO guidelines by 2020 (Ministry of Environment and Water Resources, 2014; WHO, 2006), and evaluation of this target is ongoing at the time of writing.

Air pollution comes from both city and transboundary sources (Latif et al., 2018). Studies of Singapore's air quality have affirmed regional biomass burning to be the dominant contributor to domestic pollution during intense burning years (Hertwig et al., 2015; Hyer and Chew, 2010; Koe et al., 2001; Lee et al., 2018; Mead et al., 2018; Salinas et al., 2013; Velasco and Rastan, 2015). The burning in turn is influenced by a multitude of meteorological and economic factors (Field et al., 2009; Marlier et al., 2013; Tangang et al., 2017). The focus on intense but brief burning events can neglect the role that pollution sources within Singapore play in chronic exposure. The impact of large signals from biomass burning events do not rely heavily on the local atmospheric chemistry and environment. In contrast, during "non-hazy" conditions, the spatio-temporal profile of pollutants throughout Singapore may depend on both remote and local sources. The city-state's small size results in the near co-location of different polluting sources such as ports, petrochemical refineries, power plants, light industries and downtown traffic, together with residential emissions from a population of 5.6 million inhabitants in an area of only 720 km^2.

It is advantageous to simulate the city's air quality under relatively "non-hazy" conditions, to establish a baseline against which an intense burning episode can be compared (Velasco and Roth, 2012). Air quality deterioration brought about by regional biomass burning is commonly termed as "hazy". Strictly speaking, one would expect some contribution from biomass burning emissions even under "non-hazy" conditions. Hence, an additional sensitivity simulation without biomass burning emissions was carried out, to evaluate the relative contribution of biomass burning to "non-hazy" air quality.

This report focuses on ozone (O_3) since it has been most consistently associated with health impacts (WHO, 2013). An additional pollutant monitored by the National Environment Agency (NEA), nitrogen dioxide (NO_2) is also evaluated due to its influence on O_3.

2 DATA AND METHOD

2.1 EXPERIMENTAL DESIGN

Air quality was simulated using a series of nested chemistry transport models (Fig 1a-c), termed [BASE].

The simulated surface concentrations of O_3 and NO_2 were compared to reanalysis and monitoring data, described in the "Observational data" sub-section. Another set of simulations without biomass burning emissions is termed [NOFIRE].

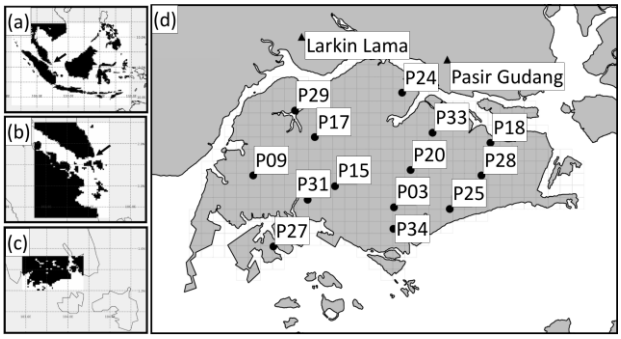

Figure 1. (a)-(c): The simulation domains used are coloured white in the map, while land-sea mask is coloured black; (a) regional, (b) sub-regional, (c) local. Arrow shows approximate location of the next nest. (d) The monitoring sites used for verification marked by circles. The grid shows the 1.4 km resolution of the local simulation.

Several criteria constrained the selection of a suitable study period: firstly, low regional biomass burning or atypical haze plumes pulled over the island by synoptic conditions; secondly, no *strong* El Niño Southern Oscillation (ENSO) extremes, to avoid the associated atypical meteorology; thirdly, availability of emission inventories for the study period. The most suitable period at the time of the study was April 2014 to March 2015, but emissions inventories were incomplete for this period at the time of the study. The next suitable period of April 2008 to March 2009 was selected for simulation. Based on these criteria, April 2008 to March 2009 was selected. The Fire Inventory from NCAR (FINN) biomass burning inventory used in this study reported 23 Tg of carbon monoxide (CO) emitted in this region (95 ˚E to 125 ˚E, 10 ˚S to 15 ˚N) during the target period. This was low compared to an average annual release of 32 Tg of CO. This period was Niña-like transitioning into the El Niño of 2010, avoiding the El Niño period of summer 2009-spring 2010 and the strong extended La Niña period of summer 2010 to spring 2012. Note the same 2008-2009 period was used during the verification of the meteorological model.

2.2 AIR QUALITY MODEL

The Community Multiscale Air Quality model version 5.2 (CMAQ; Byun and Schere, 2006) was set up using three nested domains with increasingly fine horizontal resolutions as shown in Fig. 1a-c: 35 km (regional), 7 km (sub-regional), and 1.4 km (local). The chemistry setup was the Carbon Bond Mechanism version 5 (CB05) with aerosol module version 5 (cb05cl_ae5_aq). Each parent domain provided boundary conditions for its child domain.

Boundary conditions for the outermost domain were provided by GEOS-Chem version 9-02 (Bey et al., 2001; Lam and Fu, 2009). This global simulation was performed at a resolution of 4° latitude × 5° longitude, using meteorology provided by the NASA Global Modeling and Assimilation Office from their GEOS data assimilation system.

Meteorological forcing for each CMAQ simulation was provided by the Weather Research and Forecasting model v3.3 (WRF; Skamarock et al., 2008), run with three nested domains of identical resolution. This configuration of WRF has been extensively calibrated and validated for Singapore (Li et al., 2013, 2016a, 2016b).

2.3 EMISSIONS INVENTORY

Anthropogenic gaseous and particulate air pollutant emissions were taken from the Emissions Database for Global Atmospheric Research version 4.3.1 (EDGAR; Crippa et al., 2016), of spatial resolution 0.1° × 0.1°. The emissions were in monthly mean format and monthly means of the study period were used. These emissions were adjusted to diurnal emission profiles that were based on USA and European emission inventories (Wang et al., 2007, 2010; Kannari et al., 2007; Yim et al., 2015). Source-specific chemical speciation profiles from the United States Environment Protection Agency (USEPA) SPECIATE database version 4.4 were assumed for volatile organic compounds (VOCs), $PM_{2.5}$, nitric oxide/nitrogen dioxide (NO_x), and sulphur dioxide (SO_x) emissions (USEPA, 2014; Simon et al., 2010; Li et al., 2017). Anthropogenic aviation sector emissions were calculated using the Aviation Emissions Inventory Code (AEIC v2.1; Simone et al., 2013), based on 2005 values. Biogenic emissions were estimated using the Model of Emissions of Gases and Aerosols from Nature version 2 (MEGAN; Guenther et al., 2012), and adjusted with diurnal profiles (Guenther et al., 1999). Biomass burning emissions for the simulation period were taken from the Fire Inventory from NCAR version 1.5 database (FINN; Wiedinmyer et al., 2010), at a 1 km resolution. Fire plume rise was calculated using the formulation of Briggs (1965) and fuel-specific energy fluxes of Freitas et al. (2006).

A major hindrance to high resolution modelling over the local domain was the unavailability of high resolution local emission inventories. Hence, high resolution spatial surrogates were used to downscale

global inventories to 1.4 km spatial resolution for the local simulation. Land surface transportation emissions were downscaled using road density calculated by aggregating vector data from OpenStreetMaps (available at https://planet.openstreetmap.org). Residential emissions were downscaled using population density from Landscan (Bright et al., 2012). Industrial sector emissions were downscaled using industrial land footprint, estimated by rasterizing and re-gridding the Singapore Land Authority's industrial site map, and Iskandar Malaysia's current and proposed development plans. Power generation emissions in Malaysia were downscaled to power plant locations from the Global Energy Observatory, using their type and capacities. Those in Singapore were downscaled to power plant locations from visual inspection of Google Maps satellite imagery using operating capacities deduced from their relative ratio of SO_2 emissions (NEA, 2015). The power generation emissions were distributed vertically (Wang et al., 2010). Shipping sector emissions were downscaled to aggregated ship position information (Corbett and Koehler, 2003).

2.4 Observational data

Regional observations of air quality were sparse, but records of annual mean concentrations of NO_2 were available for different cities and years from the WHO Global Urban Ambient Air Pollution Database (WHO, 2016c) and Clean Air Asia (http://cleanairasia.org/publications). Observations for the simulation period were missing at many sites due to the sparse data. For the regional simulation, the simulated range of daily mean pollutant values from the grid-point closest to the measurement site was compared against the range of these annual mean measurement values. Simulated annual mean surface concentrations of O_3 and NO_x were also compared against values from the Monitoring Atmospheric Composition and Climate (MACC; Inness et al., 2013) reanalysis at the lowest model level (~10m).The MACC reanalysis has a native resolution of 70 km.

For the local simulation, the 14 NEA monitoring sites in Singapore were used for verification (Fig. 1d). Hourly observations were provided in units of µg m^{-3}; gaseous pollutants were converted back to ppbV through division by fixed factors from NEA.

Verification of daily mean concentrations was performed separately for the two monsoons based on local climate; The Meteorological Service Singapore (2012) defines the summer monsoon as June-September (SUM), and the winter monsoon as December-March (WIN). Ranges of daily mean concentrations from the local simulation and monitoring sites were compared and considered as 'similar' (green) with an overlap of the quartile range, 'biased' (blue) with an overlap of the 10th-90th percentile range, and 'erroneous' (red) without overlap of the 10th-90th percentile range. Verification of pollutant diurnal cycle was done by comparing the ranges of hourly mean concentrations.

Both values from the grid-point in the local simulation closest to the monitoring site, as well as the mean of nine grid-points surrounding the site, were compared against the range of daily mean observations. The differences between the two methods were minor, with the mean quantity having weaker extremes. The results shown below used nine grid-point means. When calculating correlations, the five-day running mean over all sites was used to focus on the variation of pollutant level with weather patterns rather than day-to-day variations. 95% confidence intervals (C.I.) for correlation coefficients are shown in brackets behind the correlation values.

3 Results

3.1 Regional domain (35 km × 35 km resolution)

Fig. 2 shows the annual mean surface concentrations of NO_2 from the regional simulation, which were close to the median observation at available sites, with the exception of the stations in Cambodia.

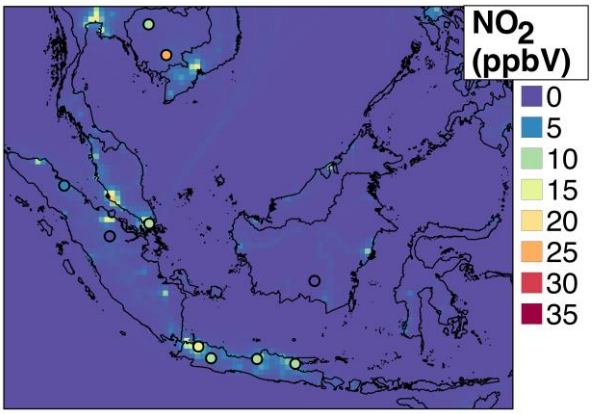

Figure 2. NO_2 surface concentrations (ppbV), comparing the annual mean from the regional simulation against medians of observed annual means when available (circles).

Fig. 3 compares annual mean surface concentrations of NO_x and O_3 from the regional simulation against the MACC reanalysis. Spatial patterns were qualitatively similar, but absolute values were different when regridded to the same resolution (not shown). O_3 was lower over Borneo Island (below 15

ppbV). The regional simulation resolved pollution patterns over major cities; high concentrations of NO_x were found over Java Island, the Strait of Malacca, and the Bangkok region. O_3 concentrations could be lower or higher over these urban areas.

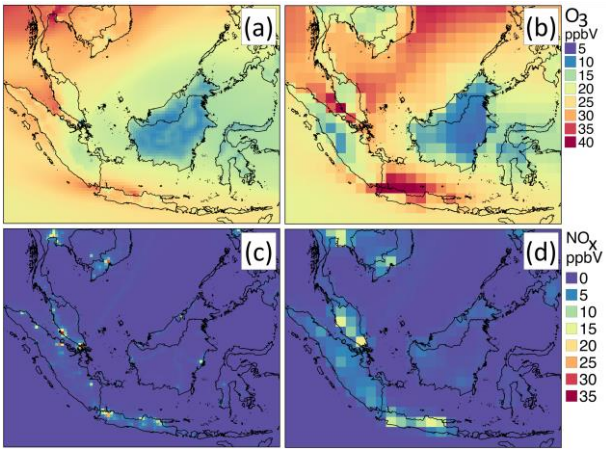

Figure 3. (a)-(b): O_3 annual mean surface concentrations (ppbV), comparing (a) regional simulation with (b) MACC reanalysis. (c)-(d) similar for NOx.

3.2 Local domain (1.4 km × 1.4 km resolution)

The site-based comparison of Fig. 4 shows good performance simulating O_3 over the island. Simulated and observed ranges were similar for all sites except Jurong Island (P27) during the winter monsoon. The correlation between simulation and observation was 0.75 (0.66 - 0.82) and 0.43 (0.27 - 0.56) during the winter and summer monsoon, respectively.

The sites measuring O_3 were a subset of sites measuring NO_2. From the site-based comparison of Fig. 5, NO_2 was better simulated during the summer than the winter monsoon; 8 of 14 sites showed similar ranges during the summer monsoon, while only 4 of 14 sites showed similar ranges during the winter monsoon. The correlation between simulation and observation was 0.28 (0.11 - 0.44) and 0.60 (0.47 - 0.70) during the winter and summer monsoon, respectively.

Spatial plots of seasonal mean surface concentrations in Fig. 5 suggest a reason for this seasonal discrepancy -- seasonal pollutant plumes downwind of power stations. O_3 concentrations were lower inside the plumes (Fig 6a-b). This should not be considered "better air quality" since NO_2 concentrations were elevated inside the plumes (Fig. 6c-d). NO_2 concentrations were better simulated when sites were outside of the plumes.

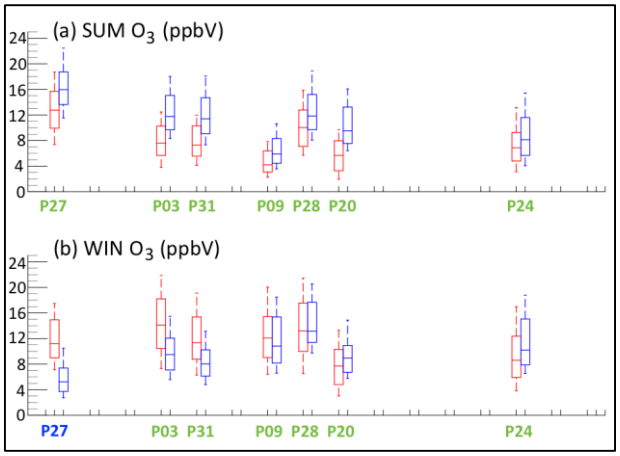

Figure 4. Daily mean surface O_3 concentrations (ppbV), comparing the local simulation (blue bars) with monitoring data (red bars), during the (a) summer monsoon and (b) winter monsoon. Bars are marked at 10th, 25th, 50th, 75th and 90th percentile values. Green, blue and red stations indicate similar, biased, and poor matches with observations, respectively (see Observational data section).

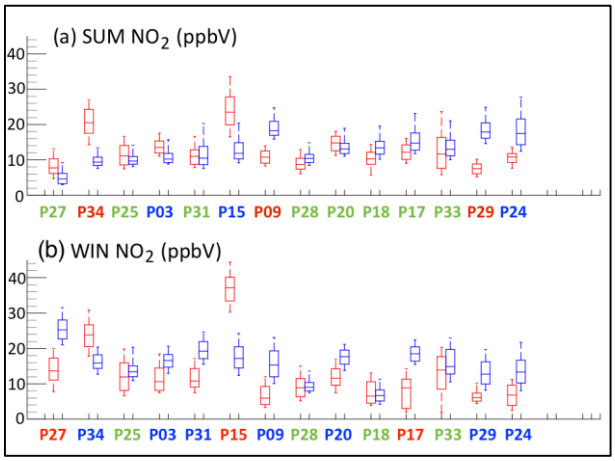

Figure 5. Similar to Fig. 4 but for NO_2 concentrations (ppbV).

We can classify the monitoring sites by visual inspection of Figure 6 as follows: Strongly affected by plumes during winter (W) or summer (S) monsoons; weakly affected by plumes during winter (w) or summer (s); outside of plumes (X). Some sites may be affected by plumes during both monsoons, but all of these sites were more strongly affected in one season. The subset of sites also recording O_3 is in bold text.

Sites strongly affected by plumes: Ws17, **Ws27**, **Ws31**, **Ws34** (both seasons); W15, **S09** (one season). Sites weakly affected by plumes: **w03**, **w20**, w33, **s24** (one season). Sites outside plumes: X18, X25, **X28**, X29.

The relative seasonal change was not as well-simulated. Observed O_3 concentrations were higher during the winter than summer monsoon, at all sites except Jurong Island (**Ws27**). The same relative change was seen in the simulations for sites that lie outside wintertime pollution plumes (**S09**, **s24** and **X28**). The

reverse change (lower wintertime) was seen at sites that lie inside those plumes (**Ws27**, **Ws31**, **w03**, **w20**). Hence, the relative seasonal change was correctly simulated at 4 of 7 sites (**Ws27**, **S09**, **s24**, **X28**).

Simulated NO_2 concentrations were higher during the winter than summer monsoon at the 7 sites affected by winter pollution plumes (Ws17, W15, **Ws27**, **Ws31**, **w03**, **w20**, w33), as well as X25. This effect of the plumes was not always observed. The relative seasonal change of NO_2 was reproduced at most sites except for 4 sites (Ws17, **Ws31**, **w03**, **w20**). All 4 sites were affected by wintertime pollution plumes.

NO_2 was best simulated at the 5 monitors on the eastern side of the island (X18, X25, **X28**, w33). The median of simulated daily mean NO_2 concentration lay within ±3 ppbV of the observed value, and the relative seasonal change was correctly simulated. The relative seasonal changes of O_3 and NO_2 were both correctly simulated in unison at **Ws27**, **S09**, **s24**, and in a sense **X28** where little change between seasons was observed.

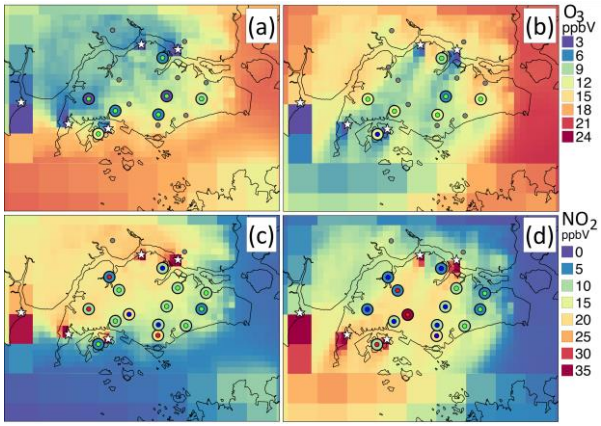

Figure 6. (a)-(b): Seasonal mean surface concentrations of O_3 (ppbV), comparing the local simulation (shading) against observations (circles), during the (a) summer monsoon and (b) winter monsoon. The local simulation is overlaid on the sub-regional simulation. Red, blue, green inner circles respectively indicate an increasing quality match between observation and model. Grey inner circles indicate stations without observations for the species. White stars indicate the locations of power stations. (c)-(d) similar for NO_2.

3.3 Diurnal Variability

Fig. 7 shows the range of hourly mean surface concentrations for O_3 and NO_2. The simulation reproduced the key features of the diurnal cycles, despite biases. The one-hour phase shift between simulated and observed diurnal cycles was expected as policy-based local time (GMT+8) is one hour ahead of what would be expected from longitude (GMT+7).

From Fig. 7a, the observed peak median O_3 concentration was ~18 ppbV at 1400-1500 local time. Day-time O_3 concentrations were well simulated in terms of both median value and interquartile range, but simulated concentrations were biased by ~5 ppbV. From Fig. 7b, the diurnal pattern of NO_2 was similarly well captured, particularly day-time values of median ~13 ppbV during 0900-1600 local time. Simulated night-time concentrations were ~5 ppbV higher than observed. This excessive night-time build-up of NO_2 was consistent with the excessive daytime O_3.

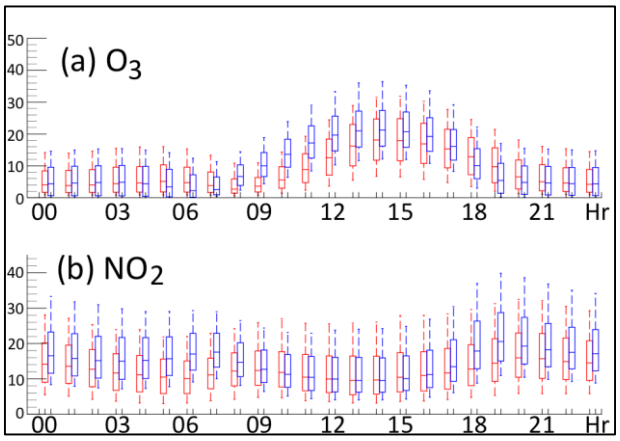

Figure 7. The diurnal cycle of hourly mean surface concentrations (ppbV), comparing the local simulation (blue bars) with monitoring data (red bars), for (a) O_3 and (b) NO_2. Bars are marked at 10th, 25th, 50th, 75th, and 90th percentile, averaged over all monitoring sites measuring that species.

3.4 Simulations without Biomass Burning

Fig. 8 shows the seasonal mean surface concentration of O_3 from the [NOFIRE] simulations as a fraction of concentrations from [BASE]. Despite the lower than normal levels of biomass burning, it had a large regional impact during the summer monsoon, specifically northwest of Borneo and over Sumatra. Simulated O_3 concentrations from [BASE] were about twice that from [NOFIRE] during the summer monsoon.

However, the impact of biomass burning on local O_3 was relatively minor during the study period; O_3 concentrations from [NOFIRE] differed from [BASE] by only about 10% or less.

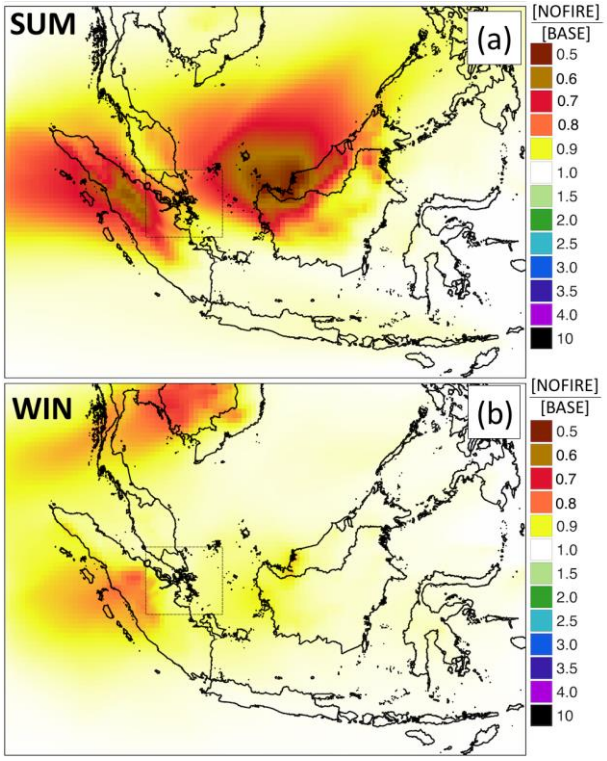

Figure 8. Seasonal mean concentrations of O_3, in [NOFIRE] as a relative fraction of [BASE], during the (a) summer monsoon and (b) winter monsoon. The sub-regional simulation is overlaid on the regional simulation.

4 Discussion

O_3 and NO_2 were best simulated at sites on the east side of Singapore, likely because these sites were relatively unaffected by pollutant plumes. At four of the sites affected by wintertime pollution plumes (**Ws27**, **Ws31**, **w03**, **w20**), the simulated increase in NO_2 from summer to winter monsoon greatly exceeded that observed, and relative seasonal change in O_3 was wrongly simulated except at **Ws27**. In contrast, sites outside the wintertime plumes correctly simulated the relative seasonal changes of both NO_2 and O_3 (**S09**, **s24**, **X28**).

The adverse effect of plumes may be caused by the over-estimation of power plant NO_x emissions during the winter monsoon. This is supported by an examination of the EDGAR inventory: Firstly, local NO_x emission was dominated by the energy and transportation sectors, and only the energy sector had a strong seasonal dependence. Secondly, the Singaporean NO_x emission for 2008 was ~30 Gg greater than (~1.25 times of) that given by another inventory, MIX.

Ws27 (Jurong Island) was particularly noteworthy. During winter, the simulation of O_3 and NO_2 was inferior. The performance of chemistry there may be different compared to the rest of Singapore, perhaps due to the presence of both power plant and major petrochemical industry.

5 Summary

The April 2008-March 2009 period, a time of low regional biomass-burning, was simulated over three nested domains using the Community Multi-scale Air Quality (CMAQ) model v5.2 with the carbon bond mechanism version 5 (CB05). Surface concentrations of O_3 and NO_2 were verified against observations from 14 Singaporean sites and found to be generally well-simulated.

Air quality at specific sites was strongly affected by downwind seasonal plumes from power plants. O_3 and NO_2 were less well simulated at these sites, particularly in terms of biases and relative seasonal variations. Due to the sizeable impact of pollution plumes, we recommend that future air quality analyses take into account seasonal chemistry along pollution plumes. In this study, the extent of the plumes was determined by visual inspection. Future work with plume models or trajectory tracking models would be able to better evaluate the extent these plumes affect different locations over the island.

We recommend future research in the local domain focused on constraining power plant emissions and chemistry inside power plant plumes. Power plants and petrochemical industries are good candidates for study due to their impact on the air quality over almost half the sites in Singapore.

6 References

Bey, I., Jacob, D.J., Yantosca, R.M., Logan, J.A., Field, B.D., Fiore, A.M., Li, Q., Liu, H.Y., Mickley, L.J. and Schultz, M.G. (2001) 'Global modeling of tropospheric chemistry with assimilated meteorology: Model description and evaluation', *J. Geophys. Res.,* 106(D19): 23073–23095. DOI: 10.1029/2001JD000807.

Briggs, G.A. (1965) 'A Plume Rise Model Compared with Observations', *Journal of the Air Pollution Control Association* 15(9): 433-438. DOI: 10.1080/00022470.1965.10468404.

Bright, E.A., Coleman, P.R., Rose, A.N. and Urban, M.L. (2012) LandScan 2011. https://landscan.ornl.gov

Burnett, R.T., Pope, C.A., Ezzati, M., Olives, C., Lim, S.S., Mehta, S., Shin, H.H., Singh, G., Hubbell, B., Brauer, M., Anderson, H.R., Smith, K.R., Balmes, J.R., Bruce, N.G.,

Kan, H., Laden, F., Prüss-Ustün, A., Turner, M.C., Gapstur, S.M., Diver, W.R. and Cohen, A. (2014), 'An Integrated Risk Function for Estimating the Global Burden of Disease Attributable to Ambient Fine Particulate Matter Exposure', *Environ Health Perspect.* 122:397-403. DOI: 10.1289/ehp.1307049

Byun, D. and Schere, K.L. (2006), 'Review of the governing equations, computational algorithms, and other components of the Models-3 Community Multiscale Air Quality (CMAQ) modeling system', *Appl. Mech. Rev.* 59(2):51-77. DOI: 10.1115/1.2128636

Clean Air Asia. http://cleanairasia.org/publications/ (last access 21 Dec 2018)

Corbett, J.J. and Koehler, H.W. (2003), 'Updated emissions from ocean shipping', *J. Geophys. Res.* 108(D20):4650. DOI: 10.1029/2003JD003751

Crippa, P., Castruccio, S., Archer-Nicholls, S., Lebron, G.B., Kuwata, M., Thota, A., Sumin, S., Butt, E., Wiedinmyer, C. and Spracklen, D.V. (2016), 'Population exposure to hazardous air quality due to the 2015 fires in Equatorial Asia', *Scientific Rep.* 6: 37074. DOI: 10.1038/srep37074

Field, R.D., van der Werf, G.R. and Shen, S.S.P. (2009), 'Human amplification of drought-induced biomass burning in Indonesia since 1960', *Nat. Geosci.* 2: 185–188. DOI: 10.1038/ngeo443

Fonseca, R.M., Zhang, T. and Koh, T.Y. (2015), 'Improved simulation of precipitation in the tropics using a modified BMJ scheme in the WRF model', *Geosci. Model Dev.* 8: 2915-2928. DOI: 10.5194/gmd-8-2915-2015.

Freitas, S.R., Longo, K.M. and Andreae, M.O. (2006), 'Impact of including the plume rise of vegetation fires in numerical simulations of associated atmospheric pollutants', *Geophys. Res. Lett.* 33: L17808. DOI:10.1029/2006GL026608

Guenther, A., Jiang, X., Heald, C.L., Sakulyanontvittaya, T., Duhl, T., Emmons, L.K. and Wang, X. (2012), 'The Model of Emissions of Gases and Aerosols from Nature version 2.1 (MEGAN2.1): an extended and updated framework for modeling biogenic emissions', *Geosci. Model Dev.* 5(6): 1471–92. DOI: 10.5194/gmd-5-1471-2012

Guenther, A., Baugh, B., Brasseur, G., Greenberg, J., Harley, P., Klinger, L., Serça, D., Vierling, L. (1999), 'Isoprene emission estimates and uncertainties for the Central African EXPRESSO study domain', *J. Geophys. Res. Atmos.* 104(D23): 30625-39. DOI: 10.1029/1999JD900391

Hansen, A.B., Witham, C.S., Chong, W.M., Kendall, E., Chew, B.N., Gan, C., Hort, M.C. and Lee, S-Y. (2019), 'Haze in Singapore – Source Attribution of Biomass Burning PM_{10} from Southeast Asia', *Atmos. Chem. Phys.* 19:5363–5385. DOI: 10.5194/acp-19-5363-2019

Hertwig, D., Burgin, L., Gan, C., Hort, M., Jones, A., Shaw, F., Witham, C. and Zhang, K. (2015), 'Development and demonstration of a Lagrangian dispersion modeling system for real-time prediction of smoke haze pollution from biomass burning in Southeast Asia', *J. Geophys. Res. Atmos.* 120:12605–30. DOI: 10.1002/2015JD023422

Hoek, G., Krishnan, R.M., Beelen, R., Peters, A., Ostro, B., Brunekreef, B. and Kaufman, J.D. (2013), 'Long-term air pollution exposure and cardio-respiratory mortality: a review', *Environ. Health* 12(1):43. DOI: 10.1186/1476-069X-12-43

Hyer, E.J. and Chew, B.N. (2010), 'Aerosol transport model evaluation of an extreme smoke episode in Southeast Asia', *Atmos. Environ.* 44(11): 1422-7. DOI: 10.1016/j.atmosenv.2010.01.043

Inness, A., Baier, F., Benedetti, A., Bouarar, I., Chabrillat, S., Clark, H., Clerbaux, C., Coheur, P., Engelen, R.J., Errera, Q., Flemming, J., George, M., Granier, C., Hadji-Lazaro, J., Huijnen, V., Hurtmans, D., Jones, L., Kaiser, J.W., Kapsomenakis, J., Lefever, K., Leitão, J., Razinger, M., Richter, A., Schultz, M.G., Simmons, A.J., Suttie, M., Stein, O., Thépaut, J-N., Thouret, V., Vrekoussis, M., Zerefos, C. and the MACC team (2013), 'The MACC reanalysis: an 8 yr data set of atmospheric composition', *Atmos. Chem. Phys.* 13 (8): 4073-4109. DOI: 10.5194/acp-13-4073-2013

Kannari, A., Tonooka, Y., Baba, T. and Murano, K. (2007), 'Development of multiple-species 1km×1km resolution hourly basis emissions inventory for Japan', *Atmos. Environ.* 41(16):3428–39. DOI: 10.1016/j.atmosenv.2006.12.015

Koe, L.C.C., Arellano Jr, A.F. and McGregor, J.L. (2001), 'Investigating the haze transport from 1997 biomass burning in Southeast Asia: its impact upon Singapore', *Atmos Environ.* 35(15): 2723–34. DOI: 10.1016/S1352-2310(00)00395-2

Lam, Y.F. and Fu, J.S. (2009), 'A novel downscaling technique for the linkage of global and regional air

quality modeling', *Atmos. Chem. Phys.* 9: 9169-9185. DOI: 10.5194/acp-9-9169-2009

Latif, M.T., Othman, M., Idris, N., Juneng, L., Abdullah, A.M., Hamzah, W.P., Khan, M.F., Nik Sulaiman, N.M., Jewaratnam, J., Aghamohammadi, N., Sahani, M., Xiang, C.J., Ahamad, F., Amil, N., Darus, M., Varkkey, H., Tangang, F. and Jaafar, A.B. (2018), 'Impact of regional haze towards air quality in Malaysia: A review', *Atmos. Environ.* 177: 28-44. DOI: 10.1016/j.atmosenv.2018.01.002

Lee, H.H., Iraqui, O., Gu, Y., Yim, S.H.L., Chulakadabba, A., Tonks, A.Y.M., Yang, Z. and Wang, C. (2018), 'Impacts of air pollutants from fire and non-fire emissions on the regional air quality in Southeast Asia', *Atmos. Chem. Phys.* 18: 6141-56. DOI: 10.5194/acp-18-6141-2018

Li, M., Zhang, Q., Kurokawa, J.I., Woo, J.H., He, K., Lu, Z., Ohara, T., Song, Y., Streets, D.G., Carmichael, G.R., Cheng, Y., Hong, C., Huo, H., Jiang, X., Kang, S., Liu, F., Su, H. and Zheng, B. (2017), 'MIX: a mosaic Asian anthropogenic emission inventory under the international collaboration framework of the MICS-Asia and HTAP', *Atmos. Chem. Phys.* 17(2):935-963. DOI: 10.5194/acp-17-935-2017

Li, X-X., Koh, T.Y., Entekhabi, D., Roth, M., Panda, J. and Norford, L.K. (2013), 'A multi-resolution ensemble study of a tropical urban environment and its interactions with the background regional atmosphere', *J. Geophys. Res. Atmos.* 118(17): 9804-18. DOI: 10.1002/jgrd.50795.

Li, X-X and Norford, L.K. (2016a), 'Evaluation of cool roof and vegetations in mitigating urban heat island in a tropical city, Singapore', *Urban Climate.* 16:59-74. DOI: 10.1016/j.uclim.2015.12.002

Li, X-X., Koh, T.Y., Panda, J. and Norford, L.K. (2016b), 'Impact of urbanization patterns on the local climate of a tropical city, Singapore: An ensemble study', *J. Geophys. Res. Atmos.* 121(9): 4386–4403. DOI: 10.1002/2015JD024452.

Marlier, M.E., DeFries, R.S., Voulgarakis, A., Kinney, P.L., Randerson, J.T., Shindell, D.T., Chen, Y. and Faluvegi, G. (2013), 'El Niño and health risks from landscape fire emissions in Southeast Asia', *Nature Clim. Change* 3: 131–6. DOI: 10.1038/nclimate1658

Mead, M.I., Castruccio, S., Latif, M.T., Nadzir, M.S.M., Dominick, D., Thota, A. and Crippa, P. (2018), 'Impact of the 2015 wildfires on Malaysian air quality and exposure: a comparative study of observed and modeled data', *Environ. Res. Lett.* 13(4): 044023. DOI: 10.1088/1748-9326/aab325

Meteorological Service Singapore (2012), 'The Weather and Climate of Singapore'. ISBN 9789810713409

Ministry of Environment and Water Resources (2014), 'Our home, our environment, our future: sustainable Singapore blueprint 2015', Ministry of the Environment and Water Resources, Singapore.

National Environment Agency (2015), 'Environment Protection Department Annual Report', National Environment Agency, Singapore.

Salinas, S.V., Chew, B.N., Miettinen, J., Campbell, J.R., Welton, E.J., Reid, J.S., Yu, L.E. and Liew, S.C. (2013), 'Physical and optical characteristics of the October 2010 haze event over Singapore: A photometric and lidar analysis', *Atmospheric Res.* 122: 555–70. DOI: 10.1016/j.atmosres.2012.05.021

Simon, H., Beck, L., Bhave, P.V., Divita, F., Hsu, Y., Luecken, D., Mobley, J.D., Pouliot, G.A., Reff, A., Sarwar, G. and Strum, M. (2010), 'The development and uses of EPA's SPECIATE database', *Atmos. Pollut. Res.* 1: 196–206. DOI: 10.5094/APR.2010.026

Simone, N.W., Stettler, M.E.J. and Barrett, S.R.H. (2013), 'Rapid estimation of global civil aviation emissions with uncertainty quantification', *Transportation Research Part D: Transport and Environment* 25: 33–41. DOI: 10.1016/j.trd.2013.07.001

Skamarock, W.C., Klemp, J.B., Dudhia, J., Gill, D.O., Barker, D., Duda, M.G., Huang, X.Y., Wang, W. and Powers, J.G. (2008), 'A Description of the Advanced Research WRF Version 3 (No. NCAR/TN-475+STR)', University Corporation for Atmospheric Research. doi:10.5065/D68S4MVH

Tangang, F., Farzanmanesh, R., Mirzaei, A., Supari, Salimum, E., Jamaluddin, A.F. and Juneng, L. (2017), 'Characteristics of precipitation extremes in Malaysia associated with El Niño and La Niña events', *Int. J. Climatol.* 37: 696–716. DOI: 10.1002/joc.5032

United States Environmental Protection Agency (2014), SPECIATE. https://www.epa.gov/air-emissions-modeling/speciate-version-45-through-40 (last access: 16 Jun 2018)

Wang, X., Jiang, W., Liu, H., Wang, Y. and Zhang, Y. (2007), 'Numerical simulation study on the effect of major industrial sources in Nanjing on urban air quality',

Research Environmental Sciences 20: 33–43. https://doi.org/10.13198/j.res.2007.03.35.wangxy.006

Wang, X., Liang, X.Z., Jiang, W., Tao, Z., Wang, J.X.L., Liu, H., Han, Z., Liu, S., Zhang, Y., Grell, G.A. and Peckham, S.E. (2010), 'WRF-Chem simulation of East Asian air quality: Sensitivity to temporal and vertical emissions distributions', *Atmos. Environ.* 44(5): 660–9. DOI: 10.1016/j.atmosenv.2009.11.011

Velasco, E. and Roth, M. (2012), 'Review of Singapore's air quality and greenhouse gas emissions: Current situation and opportunities', *J. Air Waste Manag Assoc.* 62(6): 625-41. DOI: 10.1080/10962247.2012.666513.

Velasco, E. and Rastan, S. (2015), 'Air quality in Singapore during the 2013 smoke-haze episode over the Strait of Malacca: Lessons learned', *Sustainable Cities and Society* 17: 122–31. DOI: 10.1016/j.scs.2015.04.006

Wiedinmyer, C., Akagi, S.K., Yokelson, R.J., Emmons, L.K., Al-Saadi, J.A., Orlando, J.J. and Soja, A.J. (2010), 'The Fire INventory from NCAR (FINN) – a high resolution global model to estimate the emissions from open burning', *Geosci. Model Dev.* 3: 2439–76. DOI: 10.5194/gmd-4-625-2011

The World Bank (2016). The cost of air pollution: strengthening the economic case for action.

World Health Organization (2006). WHO Air quality guidelines for particulate matter, ozone, nitrogen dioxide and sulfur dioxide.

World Health Organization (2013). Review of evidence on health aspects of air pollution – REVIHAAP project: final technical report.

World Health Organization (2016a). WHO Expert Consultation: Available evidence for the future update of the WHO Global Air Quality Guidelines (AQGs) (2016).

World Health Organization (2016b). Ambient air pollution: A global assessment of exposure and burden of disease.

World Health Organization (2016c). WHO Global Urban Ambient Air Pollution Database (update 2016)

Yim, S.H.L., Lee, G.L., Lee, I.H., Allroggen, F., Ashok, A., Caiazzo, F., Eastham, S.D., Malina, R. and Barrett, S.R.H. (2015), 'Global, regional and local health impacts of civil aviation emissions', *Environ. Res. Lett.* 10: 034001. DOI: 10.1088/1748-9326/10/3/034001

Overview of a locally-tuned Heavy Rain's Total Threat Score (TTS) tool and its recent application using satellite-derived soundings

Ryan Kang[1] and Darryl Boh[2]

[1] Seasonal and Subseasonal Prediction Branch, Department of Climate Research, Centre for Climate Research Singapore

[2] Weather Services Division, Meteorological Service Singapore

ABSTRACT

Driven by growing public demand in Singapore for better forecasts of flash floods, there is a need to issue heavy rain warnings at longer lead times. MSS conducted a local study of atmospheric morning soundings in 2013/2014 to identify potential thermodynamic parameters and severe weather indices that could be used as an early indicator of heavy rain events hours before the flash flood occurrence in Singapore. A locally-tuned Heavy Rain Total Threat Score (TTS) tool, based on a matrix of heavy rain predictors for each season (Northeast Monsoon, Southwest Monsoon and Inter-Monsoons) was developed at the end of 2014. This objective guidance tool aims to increase the forecaster's confidence in issuing a heavy rain warning earlier if the TTS score is high that day. Recently, a preliminary TTS evaluation using 'NOAA Unique Combined Atmospheric Processing System (NUCAPS)', a satellite-derived afternoon sounding from late 2018 to early 2020, was able to capture the deterioration of atmospheric conditions during heavy rain events in the late afternoon and also provide a good discrimination between heavy and non-heavy rain events. The future operationalization of the afternoon NUCAPS' TTS tool will further empower the forecasters' ability to track changes in heavy rain threat across the day.

1 INTRODUCTION

Rain-bearing weather systems in tropical regions are complex, as convective rain clouds develop rapidly and have short-life spans. The development of tropical weather is largely driven by winds, which tend to be weaker and more variable in direction in the tropics. As a result, it is difficult to give precise forecasts of onset, location and intensity of thunderstorms. Thunderstorms occur frequently in Singapore and can occasionally bring heavy rain, lightning, and sometimes hail. As part of the daily operations in the Weather Services Division (WSD) of Meteorological Service Singapore (MSS), the duty meteorologist for public weather is required to issue warnings of heavy rain if the impending thunderstorm is forecast to develop to a certain hazardous intensity and/or duration before a flash flood occurrence. The provision of the heavy rain warning is achieved by close monitoring of convective activity using real-time observation data from satellite images (primarily from Himawari-8, a geostationary weather satellite operated by the Japan Meteorological Agency), ground-based weather radar, wind profiler radar and low-level wind convergence field (from a network of automated weather stations installed in various parts of Singapore). Heavy rain warnings typically have a lead time of 15 to 30 minutes. However, driven by the growing public demand for better and timelier forecasts, there is a need to issue heavy rain warnings at longer lead times.

Previous studies (Craven and Brooks, 2004; Groenemeijer, 2005) have identified different clusters of thermodynamic parameters and severe weather indices exhibiting considerable skill in distinguishing environments of large hail/non-hail-producing thunderstorms, tornadoes (including waterspouts) and severe convective wind events in the continental United States and the Netherlands respectively. Another study (Müller, 2009) focussing on central Europe demonstrated that extreme large-scale precipitation can be properly characterised by the extremeness of selected dynamic and thermodynamic variables. Encouraged by these findings, a systematic local study of atmospheric morning soundings was conducted by MSS in 2013/2014 to identify potential thermodynamic parameters and severe weather indices that could be used as an early

indicator of heavy rain events hours before the flash flood occurrence in Singapore.

This letter describes the data and methods used to identify a matrix of locally-tuned heavy rain predictors for each season, operationalization of the heavy rain's Total Threat Score (TTS) sounding tool at the end of 2014, and more recently, a preliminary evaluation of utilizing 'NOAA Unique Combined Atmospheric Processing System (NUCAPS)', a satellite-derived afternoon sounding, as an upgrade to the TTS morning sounding tool.

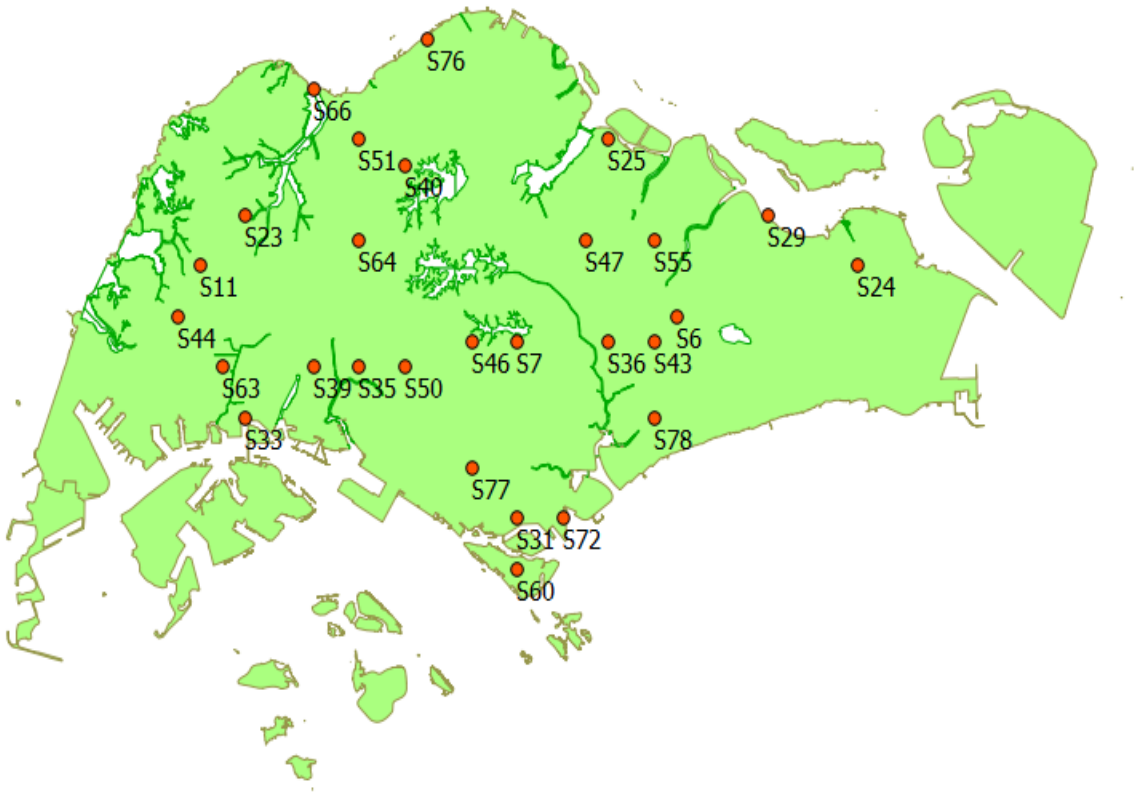

Figure 1. Map of Singapore showing the locations of the 28 rainfall stations used for climate monitoring (bottom right alpha-numbers indicate the station codes).

2 DATA AND METHODS

2.1 'Heavy Rain Event' dataset

Meteorological Service Singapore has since 1980 recorded hourly rainfall data across an island-wide network of 28 real-time automatic weather stations' (AWS) rain gauges. The distribution of stations across the island is shown in Figure 1. For this study, data from 1991 to 2012 were used to compute a multi-station daily series of "hourly rolling 2-hour total accumulated" rainfall amount. A heavy rain event is considered to have been observed for a day if the "hourly rolling 2-hour total accumulated" rainfall amount exceeds or equals 45 mm for any of the 28 AWS on that day. The rationale of using the "hourly rolling 2-hour total accumulated" rainfall amount instead of the standard "1 hour total" rainfall amount was to capture more extreme rain events that may start halfway through an hour and extend into the next hour (the duration of a thunderstorm typically ranging from ½ hour to 1½ hours). Only heavy rain events occurring from 0100UTC to 1300UTC (9am-9pm, local time) were included in the "heavy rain event" dataset for this study.

2.2 'Thermodynamic parameters' dataset from soundings

Weather balloons are launched twice daily (at 0000 UTC and at 1100UTC) at the Upper Air Observatory (UAO) located in Paya Lebar, Singapore. A

radiosonde attached to the weather balloon measures vertical atmospheric conditions (pressure, temperature, dew point, wind direction/speed) up to a height of 30 km. This sounding data can be obtained from the University of Wyoming's upper air sounding website (http://weather.uwyo.edu/upperair/sounding.html) over the same 1991-2012 period (the period of our heavy rain database). A multi-functional sounding analysis program, Universal RAwinsonde OBservation software (RAOB, http://www.raob.com) package developed by Environment Research Services (ERS) was used to process the sounding data and to generate a list of 60 thermodynamic parameters and severe weather indices (please refer to this link, http://www.raob.com/displays.php for the full list of atmospheric parameters). Only the morning soundings (at 0000 UTC) were processed as they are more indicative of any convective activity that might occur later in the day.

2.3 Selection of Predictors for heavy rain events

The selection of the most likely predictors for heavy rain events, out of the original list of 60 parameters/indices, largely followed the approaches used by Bauman (2013) and Bauman and Roeder (2014), with two modifications. Firstly, the classification of the 'heavy rain event' dataset and sounding dataset into 3 seasonal categories – 1) Northeast Monsoon, 2) Inter-monsoons and 3) Southwest Monsoon – was performed, as Singapore's weather is dominated by the Monsoons. Singapore's climate is characterised by two monsoon seasons separated by inter-monsoonal periods. The Northeast Monsoon typically occurs from December to early March, and the Southwest Monsoon from June to September. Secondly, if there was rain in the vicinity of the UAO from 2200 UTC (6 AM) to 0100 UTC (9 AM) for any day, that day was excluded from the study so as to prevent any wet sounding contamination. The numbers of the sample size (i.e. days with sounding availability and no rain in the vicinity) for the Northeast Monsoon, Southwest Monsoon and Inter-monsoons were 2336, 2204 and 2283 respectively, which was sufficient for a robust statistical analysis. The number of heavy rain days observed during the study period (and its climatological chance of heavy rain occurrence) for the Northeast Monsoon, Southwest Monsoon and Inter-monsoons were 380 (380/2336 ≈ 16%), 254 (254/2204 ≈ 12%) and 467 (467/2283 ≈ 20%) respectively.

For each of the 60 parameters, we pooled together all days with specific threshold intervals binned by either 3 to 5 indices (Very Low, Low, Moderate, High and Very High). The lower/upper thresholds of each threshold interval were largely determined by trial and error with some educated reference using the mean value and standard deviation of each

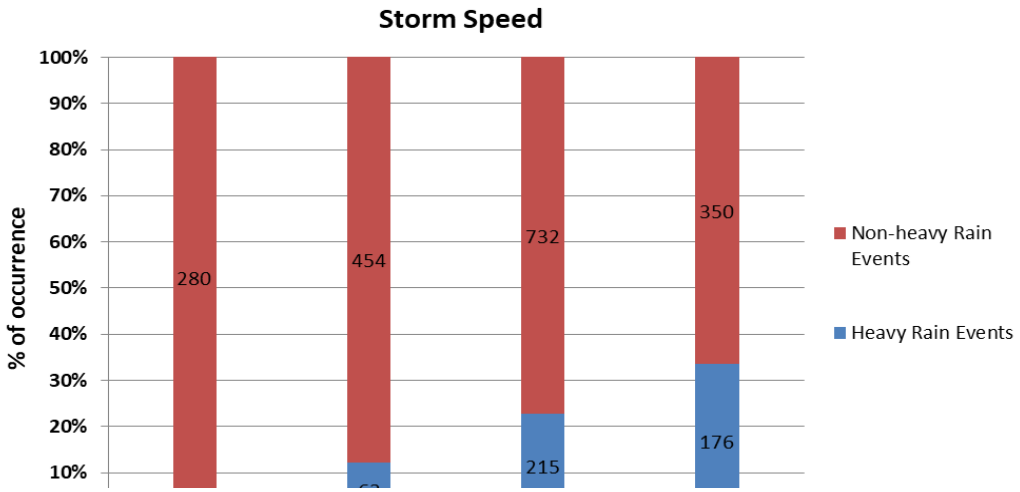

Figure 2: Stacked bar chart of "Storm Speed" parameter for the low, moderate, high and very high index in the inter-monsoon seasons. The respective number of days with reported heavy rain events (blue) and days with no reported heavy rain events (red) for each index is reflected in the coloured bars and the % of occurrence from the Y-axis.

parameter. A stacked bar chart (Figure 2) was then used to display the percentage occurrence of reported/no reported heavy rain events for each index. If there was an increasing slope of percentage of heavy rain occurrence from the lowest to the highest index in the stacked bar chart, a good heavy rain predictor was considered to have been identified. The percentages of heavy rain occurrence for the 'Low', 'Moderate', 'High' and 'Very High' index of the 'storm speed' parameter in the inter-monsoon seasons (Figure 2) are 4%, 12%, 23% and 33% respectively, and the increasing slope indicates that the 'storm speed' parameter is a good heavy rain predictor.

2.4 Total Threat Score (TTS) and Best-fit Logistic Curve

Once the predictors for heavy rain events had been identified, a 'Threat Score' (TS) was calculated by taking the difference between the percentage of heavy rain occurrence for each index of the predictor and the climatological chance of heavy rain occurrence for this monsoon (20% for inter-monsoons, 16% for Northeast Monsoon and 12% for Southwest Monsoon). As an illustration using Figure 2, the threat scores for the 'Low', 'Moderate', 'High' and 'Very High' index of the 'storm speed' heavy rain predictor are -16%, -8%, 3% and 13% respectively. A list of heavy rain predictors was identified for the three seasons and on every available sounding day, a 'Total Threat Score' (TTS) was computed by summing equally each individual heavy rain predictor's TS, normalized to a [0,100] range based on the theoretical lowest and highest possible TTS. Then, all days with the same TTS were grouped together and the chance of heavy rain for this TTS calculated as the total number of heavy rain days in this pool divided by total number of days in the same pool. The resolution of the TTS is in increments of one and we can infer from the combination method that the higher a TTS value, the higher the likelihood of a heavy rain occurrence on that day.

Using Systat Software's SigmaPlot (https://systatsoftware.com/products/sigmaplot/sp-overview/), a 5-parameter logistic (5PL) equation was used to fit the raw TTS. The 'SigmaPlot' software is able to swiftly create graphs of many complex mathematical functions, and makes data visualisation easier. The 5PL equation is characterized by its classic "S" or sigmoidal shape that fits the bottom and top plateaus of the curve and constrains the extreme ends of the curve to be within 0% to 100% (chance of heavy rain cannot be less than 0% or more than 100%).

2.5 'NOAA Unique Combined Atmospheric Processing System (NUCAPS)' dataset

NOAA Unique Combined Atmospheric Processing System (NUCAPS) (Gambacorta, 2013) utilizes the CrIS (Cross-Track Infrared Sounder) and ATMS (Advanced Technology Microwave Sounder) instruments aboard the polar orbiting Suomi-NPP satellite to retrieve vertical temperature and moisture profiles. The NUCAPS sounding has a global coverage, with a horizontal spatial resolution of 0.5 degrees. The vertical resolution varies between 1km and 4km depending on atmospheric pressure. Specifically, the derived sounding consists of 100 fixed points between 1100 mb and 0.016 mb. Suomi-NPP typically passes over the region around Singapore in the afternoon between 0500UTC and 0700UTC (1pm to 3pm Local Time), allowing our operational forecasters a chance to analyse the pre-convective atmospheric environment in the early afternoon. The NUCAPS soundings provide a unique opportunity to examine the vertical temperature and moisture profiles during the temporal gap of traditional weather balloon soundings between 0000UTC and 1200UTC. NUCAPS version 2 data calculated from Suomi-NPP can be obtained from NOAA's Comprehensive Large Array-data Stewardship System (CLASS) website (www.bou.class.noaa.gov). As a preliminary evaluation of calculating TTS using NUCAPS sounding data, the time period of September 2018 to March 2020 was used.

2.6 'Vertical wind profile' dataset from wind profiler radar

Meteorological Service Singapore has a wind profiler radar system located at the Changi Climate station. The wind profiler provides real time vertical wind information up to altitudes of 23,000 feet

depending on output power and atmospheric conditions. NUCAPS data does not contain vertical wind information, and requires supplementary wind information from the wind profiler in order to mimic the parameters measured by a radiosonde and which are required in the TTS calculation. The wind profiler dataset was extracted to match the NUCAPS dataset's time period and retrieval timing.

2.7 Modification to NUCAPS Sounding

The quality of the NUCAPS data depends heavily on local weather and cloud conditions. NUCAPS retrieval of atmospheric conditions fails when there is no radiative pathway past clouds, and hence performs poorly in overcast or precipitating cloudy conditions. Therefore, data is excluded if there is rainfall over Singapore within the hour prior to the NUCAPS retrieval timing. Secondly, due to the top of atmosphere measurement of satellite observations, NUCAPS derived temperature and moisture profiles tend to exhibit higher uncertainty and lower sensitivity to conditions in the boundary layer. Comparison between surface temperature observations at the Changi Climate Station against the temperatures derived by NUCAPS shows that NUCAPS has an average bias of -2 degrees Celsius, indicating that NUCAPS tends to underestimate temperatures near the surface. Subjective visual analysis into the sounding plots further reveal a temperature inversion below 1000 mb as a recurring feature. Singapore typically experiences strong solar heating in the day and would typically erode any near surface inversion layer. As a result of the observations above, data in the boundary layer data below 1000 mb was removed, and replaced with observed surface temperature, dew point and pressure measurements from our Changi Climate Station where the wind profiler is located as well. The combination of NUCAPS data and surface observations allows for more accurate computation of various thermodynamic parameters that rely heavily on lower level observations. Figure 3 shows an example of an unmodified NUCAPS sounding on the left and the corresponding sounding after modification on the right. Lastly, the vertical wind profile extracted from the wind profiler data was combined with the NUCAPS sounding. A total of 175 modified NUCAPS data points were extracted for this study. The modified NUCAPS sounding was then processed using the same TTS methodology as outlined above.

3 Results and Discussion

No single individual thermodynamic parameter or severe weather predictor can represent the extremity of precipitation. If a heavy precipitation event occurs, a confluence of various heavy rain predictors must be present and factor together in an accumulating manner. The curated list of heavy rain predictors (*passing the 'increasing slope of percentage of heavy rain occurrence from lowest to highest index' test in the stacked bar chart analysis)*

(a) Unmodified NUCAPS sounding (b) Corresponding sounding after modification

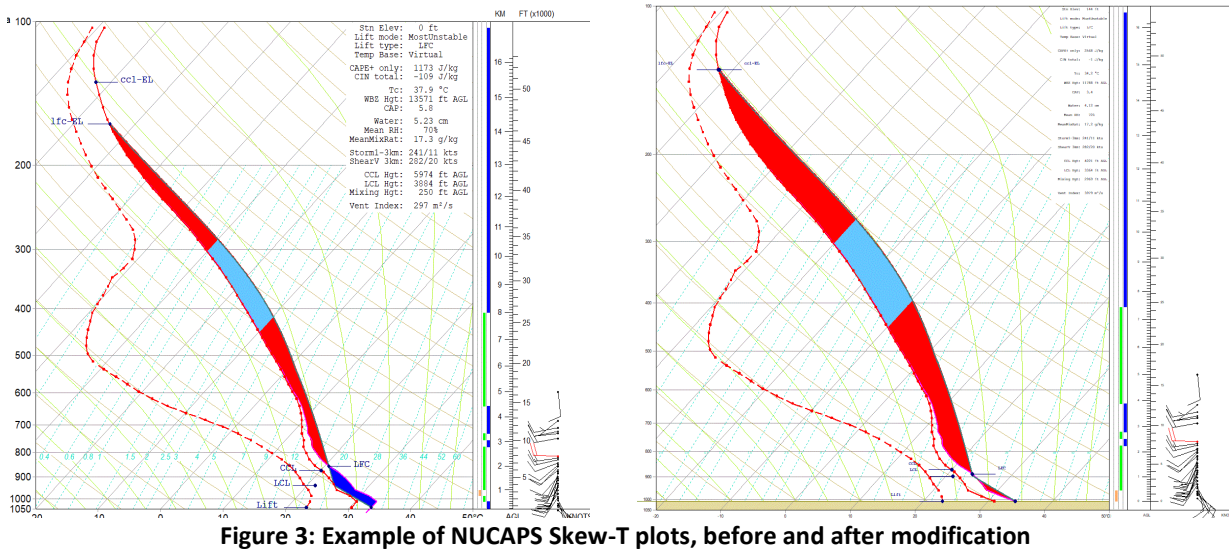

Figure 3: Example of NUCAPS Skew-T plots, before and after modification

for each of the three seasons is shown in Table 1. There are ten heavy rain predictors common to all three seasons. Please refer to the glossary for a detailed description of all the heavy rain predictors. In general, based on forecasting experience, a low steering-level wind speed (a slow-moving thunderstorm) coupled with high precipitable water (deep and moist atmospheric conditions) will have a higher chance of causing a localised heavy rain event as compared to fast-moving, passing showers. These two parameters (steering-level wind speed and precipitable water) are unsurprisingly good heavy rain predictors for all times of the year. Let us now turn our attention to the 700-500 (mid-level) lapse rate which is a good heavy rain predictor during the Southwest Monsoon only (Table 1 and Figure 4). For this lapse rate predictor, it appears counter-intuitively that a more stable mid-level lapse rate is more likely to predict a heavy rain event than an unstable mid-level atmosphere. Late morning and early afternoon thunderstorms are common during the Southwest Monsoon. A stable mid-level lapse rate may act as a capping inversion to delay/suppress convective activity until later in the day and allow for a larger build-up of low-level moisture/updrafts, resulting in more explosive thunderstorm development once the cap is broken. More in depth discussion of the physical processes/relationships for all other heavy rain predictors is beyond the

Inter-Monsoons	Northeast Monsoon	Southwest Monsoon
Steering-level Wind Speed (900hPa to 700hPa)		
Precipitable Water		
K-Index		
Shear Speed (surface to 700hPa)		
Mean-mixing Ratio (surface to 950hPa)		
Relative Humidity (surface to 750hPa)		
Wet-Bulb Zero Height		
Jefferson Index		
Mid-level Dry Slot X Mid-level Wind Speed (7000 to 20,000ft)		
Dry Slot (surface – 7000ft)		
Cross Totals	Cross Totals	700-500 Lapse Rate
	CAPE (most unstable)	CAPE (most unstable)
	Lifted index	Vorticity Generation Parameter

Table 1: The list of heavy rain predictors identified for each season. Predictors common to all three seasons are in the first ten rows.

(a) Inter-Monsoons (b) Northeast Monsoon (c) Southwest Monsoon

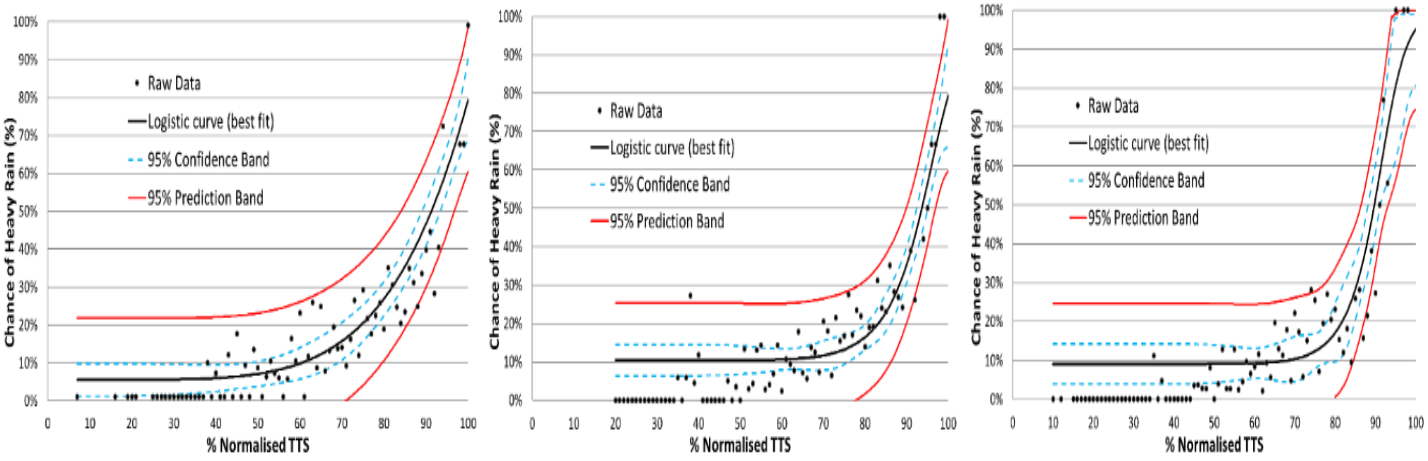

Figure 4: Best-fit logistic curves (black line) for each of the three seasons.

scope of this letter but can be investigated in future attribution studies.

The unification of heavy rain predictors (with equal weighting and calibrated with individual seasons' climatological chance of heavy rain) into a TTS enables a quick and objective assessment of the chance of heavy rain based on a single number. Logistic curve-fitting of raw TTS against chance of heavy rain (%) for each of the three seasons is shown in Figure 4. The higher the TTS value, the higher the likelihood of a heavy rain occurrence on that day. The TTS logistic curve (black lines, Figure 4) can be used to estimate the likelihood of a heavy rain event for each day against the climatological chance of heavy rain for that season. For example, the TTS for the climatological chance for inter-monsoon (20%), Northeast Monsoon (16%) and Southwest Monsoon (12%) seasons are 75, 80 and 74 respectively. If the TTS for a day in the inter-monsoon season is 90, it corresponds to a 45% chance of heavy rain occurrence (twice as likely as the normal 20%). Thus, during the inter-monsoon season, we could confidently issue a heavy rain warning earlier with a longer lead time of more than 30 minutes when the TTS is greater than 90 and the 3G wind vectors show persistent localised convergence on that day. Future research work could involve a dimension reduction analysis (e.g. Principal Component Analysis) so as to determine

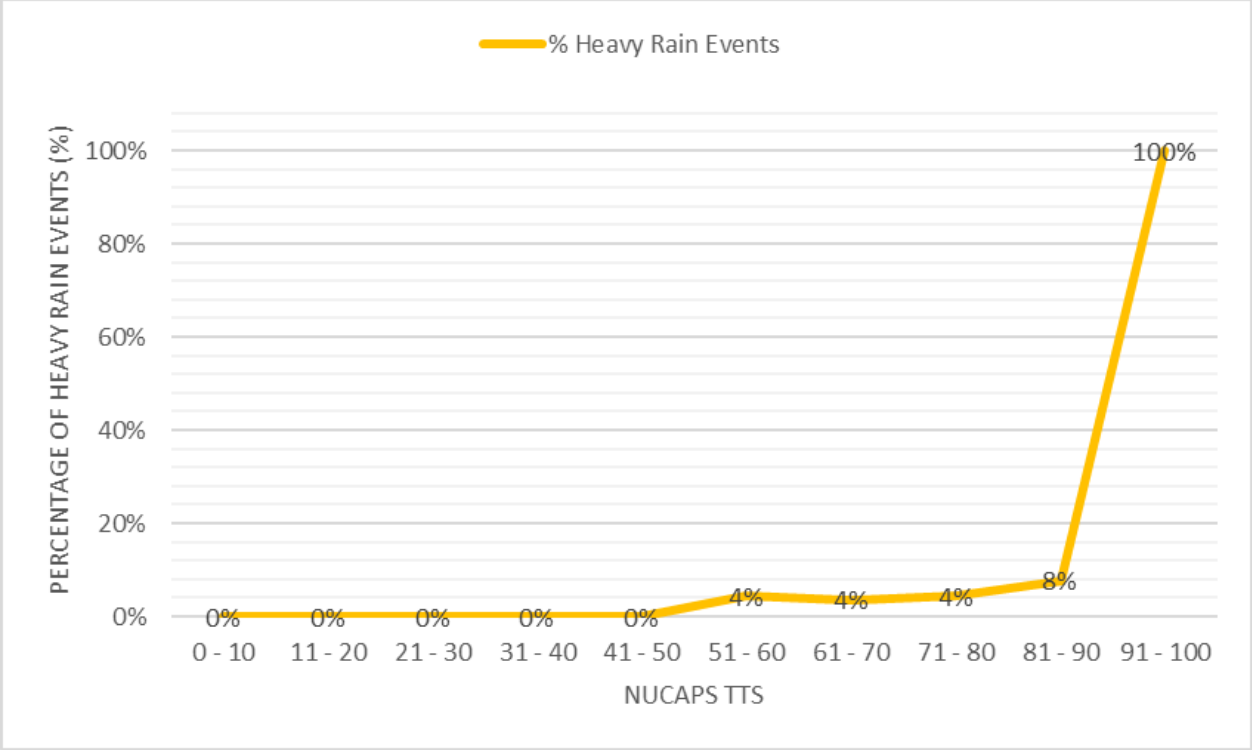

Figure 5: NUCAPS TTS against percentage chance of heavy rain events.

	Heavy Rain Events		Non-heavy Rain Events	
	Radiosonde TTS	**NUCAPS TTS**	**Radiosonde TTS**	**NUCAPS TTS**
Average	**73.6**	**82.2**	**62.8**	**65.6**
SD	**13.9**	**21.2**	**17.4**	**18.8**

Table 2: Average and Standard Deviation of morning radiosonde TTS and afternoon NUCAPS for heavy and non-heavy rain events.

which heavy rain predictor is more correlated and to give each predictor an appropriate weight instead of applying an equal weight for all heavy rain predictors.

In addition to TTS calculated from traditional weather balloon soundings, the NUCAPS TTS was calculated for a dataset of 175 data points between September 2018 and March 2020. Out of these 175 data points, there were 12 heavy rain events. The NUCAPS TTS for heavy rain events (M = 82.2, SD = 13.9) compared to the NUCAPS TTS for non-heavy rain events (M = 65.4, SD = 17.7) was significantly higher, $t(14) = 2.1$, $p = 0.001$. The smaller dataset rendered seasonal analysis ineffective. Instead, NUCAPS TTS for all seasons were categorized into bins of 10, and the percentage of heavy rain events that occurred in each bin were plotted in order to examine the general trend. Figure 5 shows an increasing trend in heavy rain events as TTS increases. The sharp increase in percentage of heavy rain events to 100% when the NUCAPS TTS exceeded 90 might not be statistically significant as there were only 5 data points. When more data points become available over time, further evaluation will be conducted.

The morning radiosonde TTS and the afternoon NUCAPS TTS for the same dates were compared for heavy and non-heavy rain events. Table 2 shows that for non-heavy rain events, the average TTS values were largely similar with a mean increase of 2.8. In contrast, there was a mean increase of 8.6 for days with heavy rain events. Most of these heavy rain events occurred between 0800UTC and 1100UTC (4pm to 7pm Local Time) and the results suggest that as atmospheric conditions developed throughout the day, NUCAPS TTS managed to capture the elevated threat in the afternoon for days with heavy rain events. These results tally, on average, with another verification of morning TTS skill scores that was done for heavy rain events from 2013 to 2016 (results not shown here) where a morning TTS filter of 80 was not able to capture some of the heavy rain events happening after 2pm local time, indicating that the atmospheric conditions may have deteriorated since the release of the morning soundings.

3.1 Operationalisation of the TTS tool

A web-based TTS tool was operationalised in November 2014. The program automatically retrieves daily sounding data and passes it to RAOB for the processing of the sounding and generation of a list of thermodynamic parameters and severe weather indices. Then, using the pre-defined predictor list of heavy-rain events (Table 1) for each of the three seasons (inter-monsoons, Northeast Monsoon and Southwest Monsoon), a 'Threat Score' is computed for each predictor and a 'Total Threat Score' for the sounding. The results are output as a .csv and presented in a more user-friendly web-based format before 9am LT daily.

Operational forecasters can access the web-based TTS tool (Figure 6) after 9am LT daily. A 5-day trend of daily TTS is displayed on the top row for the evaluation of general weather conditions over the last few days. Next, detailed information regarding very low, low, moderate, high, and very high severe thresholds for each heavy rain predictor is provided as a reference for the user. Specific values derived from the current sounding (10 September 2020 in this case) are then used to compute the individual heavy rain predictors' threat level. Forecasters can assess each predictor's threat level separately based on their level of understanding, or just use the TTS directly. The TTS on 10 September 2020 is 81 (corresponding to a 17% chance of heavy rain event occurrence), indicating a slightly elevated risk of heavy rain event occurrence as compared to the climatological chance of 12%. As a precaution, forecasters should take note of a possible artificially high TTS whenever there is shower or thunderstorm activity in the UAO vicinity in the early morning, and apply appropriate judgement during the heavy rain warning issuance decision process. Efforts are also currently underway to operationalise the afternoon NUCAPS' TTS, as an upgrade of the morning TTS tool.

For Southwest Monsoon Season Select other Seasons

5 days trend (Click here for more details)

	06-Sep-2020	07-Sep-2020	08-Sep-2020	09-Sep-2020	10-Sep-2020
TTS	72	85	78	80	81

Worst case scenario (heavy rain event 40 km radial from central Singapore) is **36%**.

Best case scenario (heavy rain event 40 km radial from central Singapore) is **2%**.

Climatological chance of heavy rain event during Southwest monsoon is **12%**.

10-Sep-2020	Thresholds			(Parameters in decreasing order of imp)			
Parameters	Very Low	Low	Moderate	High	Very High	This Sounding	Threat
Mean RH (%)	< 65	65 to 70	70 to 78	78 to 85	> 85	84	[High]
Water (cm)	< 4.5	4.5 to 5.1	5.1 to 5.6	> 5.6		6.01	[High]
Storm Speed (knots)	> 15	10 to 15	5 to 10	< 5		5	[Moderate]
Vorticity Generation Potential (VGP)	> 0.6	0.33 to 0.6	0.19 to 0.33	< 0.19		0.455	[Low]
K-Index	< 28	28 to 32	32 to 35	> 35		33	[Moderate]
Jefferson Index	< 24	24 to 28	28 to 31	> 31		29	[Moderate]
700-500 Lapse Rate (degC/km)	< -6.3	-5.7 to -6.3	-5.1 to -5.7	> -5.1		-5.5	[Moderate]
WBZ Height (feet)	< 12000	12000 to 13000	13000 to 14500	> 14500		15347	[High]
MMR (g/kg)	< 15	15 to 16	16 to 19	> 19		19.4	[High]
Shear Speed (knots)	> 25	15 to 25	5 to 15	< 5		4.7	[High]
CAPE (J/kg)	< 600	600 to 2100	2100 to 3900	> 3900		4281	[High]
Mid-level DS*Wind(7000ft-20000ft)	> 2500	600 to 2500	< 600			0	[Moderate]
Low-level Dry Slot(<7000ft)	> 25	0.01 to 25	< 0.01			0	[Moderate]

0 Missing parameters: nil

Figure 6: Screenshot of the web-based TTS tool (for Southwest Monsoon) taken on 10 September 2020, close to 6 years of operation. On this day, the computed TTS is 81, with a '95% prediction' band of 2% - 36% chance of heavy rain event occurrence. The climatological chance of heavy rain event during the Southwest Monsoon is 12% (reference period 1991 to 2012).

4 CONCLUSION

The TTS tool is a locally tuned tool to predict the probability of heavy rain events using a 22-year climatological database from the 0000 UTC (8am LT) radiosonde soundings. A proper selection of thermodynamic parameters and severe weather indices can improve the forecaster's ability to identify days with a 'heavy rain event' threat, through a more objective assessment of the daily total threat scores (TTS). The development of NUCAPS soundings further empowers the forecasters' ability to track changes in heavy rain threat across the day. This guidance tool aims to

increase forecasters' confidence in issuing a heavy rain warning earlier with a lead time of 30-45 minutes before any flash flood occurrence if the TTS score is high for that day. However, this tool only indicates if the general conditions are conducive to severe weather events. The actual location and timing of the heavy rain events will be influenced strongly by low-level boundary interactions, such as sea breeze fronts and meso-scale convergence. To address these challenging location-specific and actual timing issues of a heavy rain event, MSS' operational SINGV-DA based on the Met Office Unified Model (convective-scale numerical weather prediction system developed in-house specifically for Singapore and the surrounding region) would be a better/more timely heavy rain warning forecast solution, especially with continued model developments and improvements. In turn, the SINGV-DA prediction system can generate these model-based heavy rain event predictors, and serve as a diagnostic comparison with the observation values derived from radiosonde or satellite soundings.

Future work may involve the launching of experimental afternoon radiosonde soundings to calibrate and ground-truth the satellite-derived soundings. The main advantages of satellite-derived soundings are the spatial and temporal resolution of the product over a single radiosonde point and if done properly, the corrected satellite-derived sounding information can be assimilated into a radar-based extrapolation/SingV-DA Quantitation Precipitation Forecast (QPF) for a more accurate, timely and location-specific operational heavy rain warning system.

5 ACKNOWLEDGMENTS

The authors would like to thank their supervisors Mr Chiam Keng Oon, Mr Cheong Wee Kiong, and Mr Li Ka Wing for their guidance and operational meteorologists at MSS for their feedback in the preparation of this research letter.

6 REFERENCES

Bauman, W.H., III. (2013), 'Severe weather tool using 1500 UTC Cape Canaveral Air Force station soundings', NASA/CR-2013-217920.

Bauman, W.H. III. and Roeder, W.P. (2014), 'A tool to predict the probability of summer severe weather in east-central Florida', *Journal of Operational Meteorology*, Volume 2, No.8:89-102. http://dx.doi.org/10.15191/nwajom.2014.0208

Craven, J.P. and Brooks, H.E. (2004) 'Baseline climatology of sounding derived parameters associated with deep, moist convection', *National Weather Digest*, 28:13-24.

Gambacorta, A. (2013), 'The NOAA unique CrIS/ATMS processing system (NUCAPS): Algorithm theoretical basis documentation', NOAA Center for Weather and Climate Prediction (NCWCP), Version 1.0.

Groenemeijer, P. (2005), 'Sounding-derived parameters associated with severe convective storms in the Netherlands', Institute of Marine and Atmospheric research Utrecht, Master's thesis.

Heng, B.C.P. and Huang, X.Y. (2020), 'Verification of SINGV-DA forecasts over Singapore (December 2018 to November 2019)', *MSS Research Letters*, Issue 5:5-14.

Iturbide-Sanchez, F., da Silva, S.R.S., Liu, Q., Pryor, K.L., Pettey, M.E. and Nalli, N.R. (2018), 'Toward the Operational Weather Forecasting Application of Atmospheric Stability Products Derived from NUCAPS CrIS/ATMS Soundings', *IEEE Transactions on Geoscience and Remote Sensing*, Volume 56, No.8:4522-4545. DOI: 10.1109/TGRS.2018.2824829

Müller, M., Kašpar, M., Řezáčová, D. and Sokol, Z. (2009) 'Extremeness of meteorological variables as an indicator of extreme precipitation events', *Atmospheric Research*, 92:308-317. 10.1016/j.atmosres.2009.01.010

Nalli, N.R., Liu, Q., Reale, T., Tan, C., Sun, B., Barnet, C.D., Gambacorta, A., Tilley, F., Iturbide-Sanchez, F., Wilson, M., Sharma, A.K. and King, T. (2016), '352. Validation and Long-Term Monitoring of the Operational SNPP NUCAPS Sounding Products'. Conference paper, 96th American Meteorological Society Meeting.

Taylor, N.M. (1999) 'Climatology of sounding parameters identifying the potential for convective

storm development over central Alberta', University of Alberta, Master's Thesis. https://doi.org/10.7939/R3RX93M73.

Wheeler, A., Smith, N., Gambacorta, A., Barnet, C.D. and Goldberg, M. (2018), 237. "Evaluation of NUCAPS Products in AWIPS-II: Results from the 2017 HWT", Extended abstract for a poster (#237) presented at the 98th American Meteorological Society (AMS) Annual Meeting, Austin, TX, 7-11 January 2018.

Characterising wet and dry spells within monsoon seasons over the Malaysian peninsula and Singapore

Marcus Lim Kian Yew[1, 2] and Venkatraman Prasanna[1]

[1] Department of Climate Research, Centre for Climate Research Singapore
[2]Nanyang Technological University

ABSTRACT

This study investigates active (wet) and break (dry) spells or cycles of precipitation in the observation (uses multiple data sources for analysis; both in situ and satellite merged products) within a season: with a focus on both monsoon Seasons (SW & NE) and inter-monsoon seasons (IM1 & IM2). The wet and dry spells are further divided into short and long spells. The trends of short and long dry and wet spells are studied with available length of multiple datasets and further the impact of El Nino and La Nina conditions on the wet and dry spells are elucidated with the available datasets. Although, we noticed a decreasing trend of wet spells and an increasing trend of dry spells, the results were not significant due to the small number of years of observational data.

1 INTRODUCTION

Singapore and the Malay peninsula experience a wet tropical climate, which supports evergreen forest and large human habitations. Prolonged periods of dry (break) or wet (active) conditions affect the flora and fauna and people of this region. A huge urban population resides in this region and relies on the monsoon seasons to provide water for day-to-day activities (Fong, 2012). Prolonged torrential rains and drought can lead to disruption in the economy of the region and its trade partners.

This study identifies the characteristics of dry and wet spells within each monsoon season, using the following observed in-situ and space-based rainfall products (Cheong et. al, 2018): the Aphrodite (gauge observed) precipitation product, CHIRPS (gauge + infra-red (IR) merged) and TRMM 3B42 Satellite (microwave + infra-red (IR) sensors). Documenting dry and wet cycles from multi-decades of observations will help in the understanding of the variability of wet and dry cycles occurring within a season over the Singapore and Malay Peninsula region, thereby reinforcing results from similar studies over South Asia (Prasanna, 2016).

This work investigates active (wet) and break (dry) cycles of precipitation in the observation (data analysis) within each monsoon season, with a focus on both the Southwest (SW) and Northeast (NE) monsoon seasons and the two inter-monsoon seasons (IM1 & IM2). The four seasons are identified using previous studies of weather regime over Singapore and the Malaysian peninsula (He, 2018; Hassim and Timbal, 2019).

2 DATA AND METHOD

Three gridded precipitation datasets were used to identify wet and dry spells. The Asian Precipitation-Highly-Resolved Observational Data Integration Towards Evaluation of Extreme Events (APHRODITE-2) provides daily grid precipitation data over the Asian land region, with a high spatial resolution of 0.25° x 0.25°, based on observational rainfall data. APHRODITE-2 applies a time adjustment in order to resolve conflicting “End-of-Day” measurements, an improvement over its predecessor, APHRODITE (Yatagai et al., 2012). APHRODITE-2 v1901 was released in 2019. Climate Hazards Group InfraRed Precipitation V2.0 (CHIRPS) is a high-resolution gridded precipitation dataset which is available at a daily time scale, with a spatial resolution of 0.05° x 0.05° (Funk et al., 2015). CHIRPS is built upon a global 0.05° precipitation climatology and incorporates gridded precipitation estimates from cold-cloud estimates, station data and satellite measurements from 1981-present. The Tropical Rainfall Measuring Mission (TRMM) precipitation product was designed to measure precipitation in the tropics (Huffman et al., 2007). TRMM 3B42 with a spatial resolution of 0.25° x 0.25° provides a 3-hourly accumulated precipitation product, measured using satellite sensors (Infra red [IR] + TRMM microwave imager [TMI] + Precipitation radar [PR]) and is adjusted or bias corrected to the monthly gauge observation rainfall totals. TRMM 3B42 V7 has been recording data since December 1997.

Precipitation data from 28 meteorological stations in Singapore was spatially averaged over pre-determined domains (see below) to obtain a domain-averaged precipitation time series for the years 1998-2015.

We defined three regions for study as follows:

1) Maritime Continent region (D1): latitude 90°E – 130°E, longitude 10°S – 10°N
2) Indonesia-Malaysia region (D2): latitude 96°E – 108°E, longitude 4°S – 7°N
3) Singapore region (D3): latitude 103.5°E – 104.1°E, longitude 1.2°N – 1.5°N

The data was partitioned into 4 seasons based on the climatological onset and demise outlined in He (2018):

1) Northeast Monsoon: 5th December - 8th April
2) Inter Monsoon 1: 9th April - 12th June
3) Southwest Monsoon: 13th June - 19th October
4) Inter Monsoon 2: 20th October - 4th December

In order to determine the robustness of Aphrodite-2, CHIRPS and TRMM datasets when compared with each other, we inter-compared various statistics (correlation, seasonal mean, standard deviation) of the seasonal rainfall climatology obtained from each dataset for each season. Data between the years 1998-2015 in Aphrodite-2, CHIRPS and TRMM were selected for the inter-comparison. This time period was chosen since the TRMM dataset is only available from December 1997 onwards.

The daily spatially-averaged precipitation over land was first calculated from each of the datasets, for the Singapore region (D3) and the Indonesia-Malaysia region (D2). As the TRMM dataset provides precipitation data over both land and ocean, the dataset was first masked using a land-sea mask and only land points in the TRMM dataset were considered in the following calculations. No such land-sea mask was required for Aphrodite-2 and CHIRPS since they provide precipitation over land masses only. The Pearson's correlation coefficient was then calculated to determine the correlation between the spatial averages from the Singapore region and the Indonesia-Malaysia region (Figure 1). Note that in the seasonal correlation analysis, the daily spatially averaged precipitation for each day within each season were first added together. In order to observe the variability of the precipitation within the Indonesia-Malaysia region and to find out which region within the D2 box contributed to its overall variability, the spatial average was correlated spatially with the rainfall at each grid point in D2 using the same data sources (Figure not shown). The correlation coefficients between the averaged precipitation computed from 28 Singapore rain gauge observations and the D1 spatial precipitation average from Aphrodite, CHIRPS and TRMM for the years 1998 – 2015 were also calculated (Figure 2).

For D2, we further computed the standardised precipitation anomaly, expressed as the difference between the domain averaged daily (land) precipitation and the climatological daily precipitation mean averaged over the years 1998-2015, divided by the standard deviation of the time series from 1998-2015.

The data was categorized into 4 categories: Short wet spells, long wet spells, short dry spells and long wet spells.

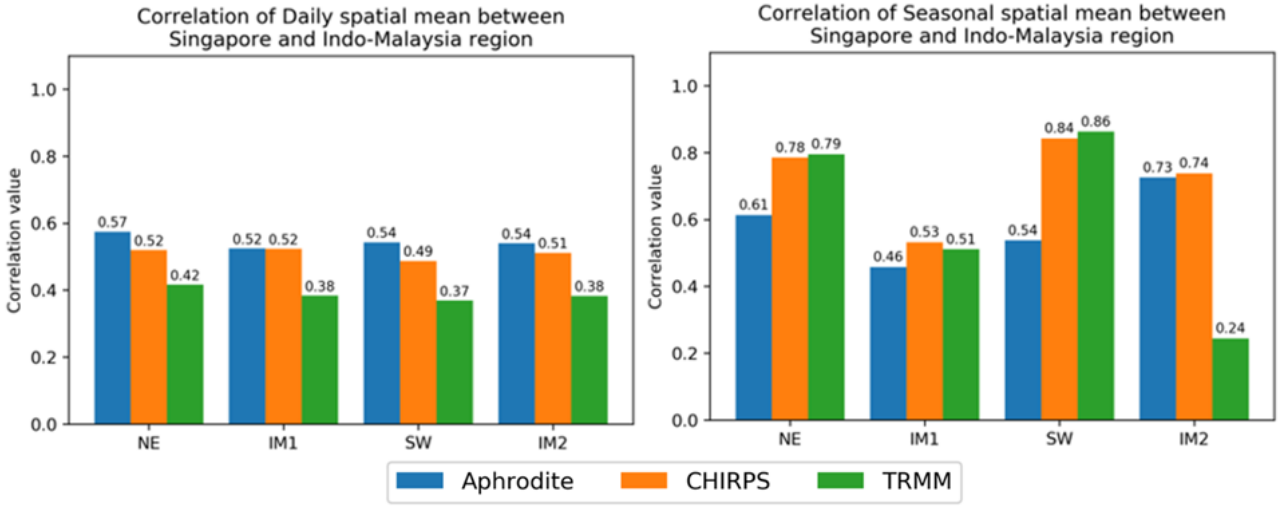

Figure 1: Barplots displaying correlation of daily spatial precipitation mean (left), seasonal spatial precipitation mean (right) between Singapore and the Indonesia-Malaysia region for each precipitation product for individual seasons

1) Short wet spells: exactly 3 consecutive days where the standardised precipitation anomaly > 0.5 SD.
2) Long wet spells: ≥ 7 consecutive days where the standardised precipitation anomaly > 0.5 SD.
3) Short dry spells: 3 consecutive days where the standardised precipitation anomaly < - 0.5 SD.
4) Long dry spells: ≥ 7 consecutive days where the standardised precipitation anomaly < - 0.5 SD.

The CHIRPS dataset which, with data spanning the years 1981-2017, was the longest dataset available to us, was used for obtaining longer term trends. CHIRPS precipitation data was used for selecting 8 El-Niño years (1982, 1986, 1991, 1994, 1997, 2002, 2009, 2015) and 8 La Niña years (1984, 1988, 1995, 1998, 2008, 2010, 2011, 2016), as outlined by Turkington et. al (2018). Wet and dry spells, both short and long, were classified by applying the same conditions above.

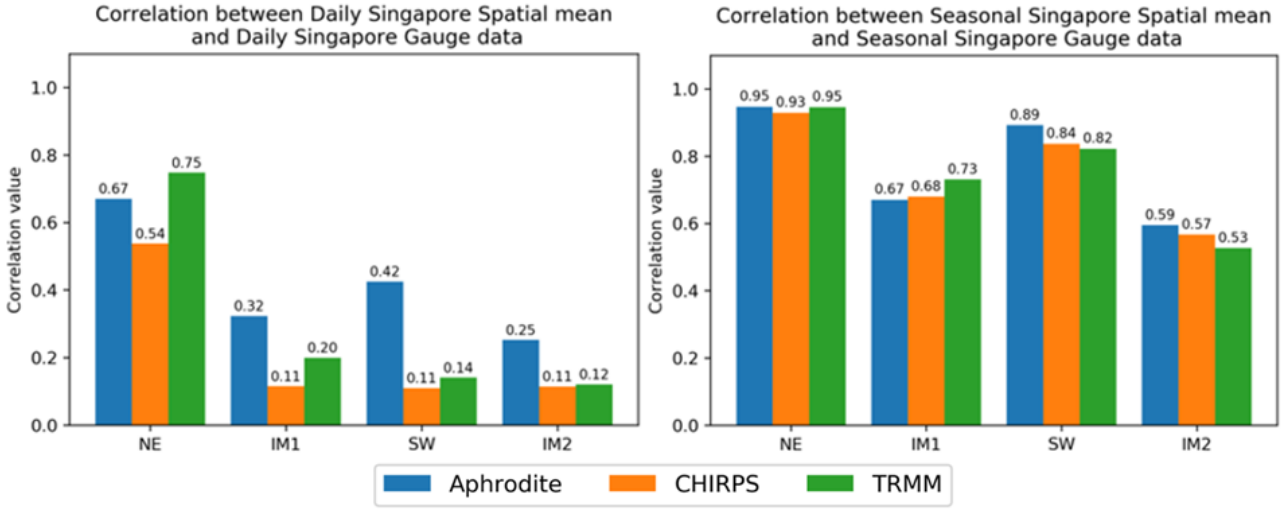

Figure 2: Barplots displaying correlation of daily spatial precipitation mean (left), seasonal spatial precipitation mean (right) between each precipitation product and the daily mean precipitation calculated from gauge data in Singapore for individual monsoon seasons.

3 Results and Discussion

The correlations between the daily spatial average precipitation of the Indonesia-Malaysia region and the Singapore region were low for all three datasets (0.37-0.57; Figure 1). This correlation improved across all seasons when the seasonal averages were used, the only exception being the seasonal correlation obtained using the TRMM dataset in IM2 (0.24) and to a lesser degree the correlation computed using the Aphrodite dataset in IM1 (0.46). Hence, utilizing the spatially averaged precipitation over the Indonesia-Malaysia region as a precipitation index may represent the variability of the precipitation over Singapore reasonably well on a seasonal time scale (0.24-0.86) but not on a daily time scale (Figure 1).

On a daily timescale, the precipitation index produced from spatially averaging the rainfall in the Indonesia-Malaysia region using Aphrodite, CHIRPS and TRMM showed poor correlations with the spatial average obtained from the precipitation time series obtained from averaging rain gauge measurements from 28 meteorological stations in Singapore. For the correlations of seasonal means, correlations exceeded 0.5 for all monsoon seasons in all datasets (0.53-0.95). Correlation for daily means only exceeds 0.5 in the NE monsoon (0.75). On a seasonal timescale, spatially averaging either Aphrodite, CHIRPS or TRMM represented the observed variability of the precipitation over Singapore well, but the data failed to capture the precipitation variability on a daily time scale, except during the NE Monsoon across the three datasets (0.11-0.75; Figure 2).

While the spatial distribution of precipitation remained similar among the three datasets, the Aphrodite data captured smaller amounts of rainfall in all regions compared to CHIRPS and TRMM (Figure 3). Consistent with the area averaged mean daily precipitation per season over the D1, D2 and D3 domains, the Indo-Malaysia region (i.e D2 domain) experienced the highest mean daily precipitation in IM2 (Figure 4).

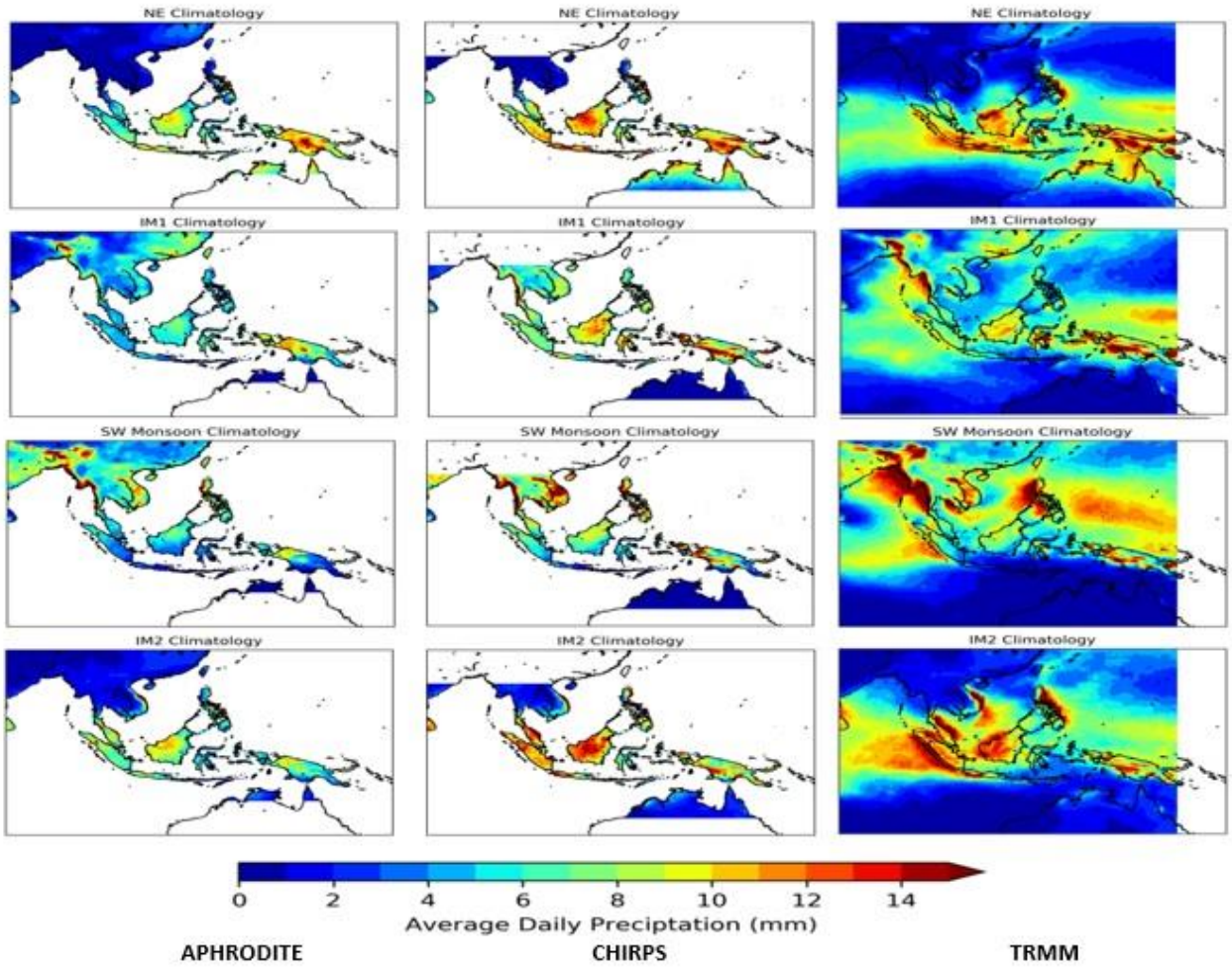

Figure 3: Climatological mean daily precipitation for individual monsoon seasons computed from Aphrodite, CHIRPS and TRMM 3B42. Refer to the main text for the definition of the seasons. The climatology was computed using data between 1998 – 2015.

Mean daily precipitation differed from season to season, with IM2 showing the highest mean daily precipitation, and SW showing the lowest mean daily precipitation across all the three data sets over the D2 domain (Figure 4). Mean daily precipitation did not differ much between CHIRPS and TRMM for all seasons, while Aphrodite gave consistently lower mean daily precipitation compared to

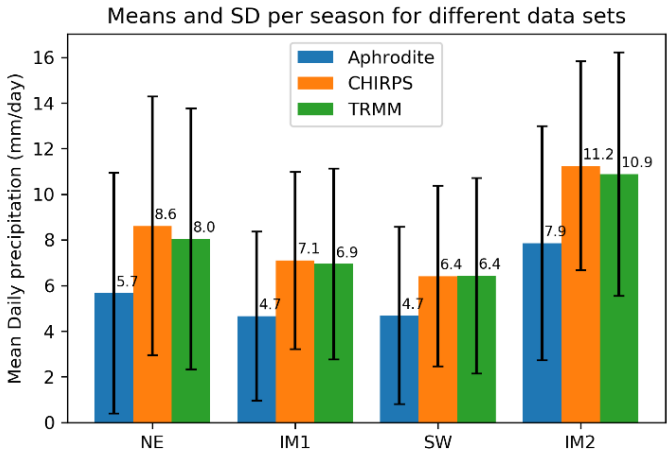

Figure 4: Mean daily precipitation and standard deviation per season obtained from each precipitation product for the D2 domain.

CHIRPS and TRMM for all seasons. The magnitudes of the standard deviation were similar across data sets on a seasonal timescale.

From Figure 5, we note that there were fewer wet spells than dry spells, whether short or long, in the Indonesia-Malaysia region from 1998 to 2015. The ratio of long spells to short spells was higher for dry spells than wet spells. Generally, the three data sets agreed in the number of short and long spells across the seasons, with some exceptions. CHIRPS reported twice the number of long wet spells (25) compared to Aphrodite (12) and TRMM (11) during the NE monsoon and reported a different number of long dry spells during IM1 and IM2 (30 and 10), being noticeably lesser than both Aphrodite (62 and 34) and TRMM (62 and 20) during long dry spells.

Figure 5 shows the differences among the datasets for short and long wet and dry spells for each season. In order to analyse the long-term trend of wet and dry spells in the Indonesia-Malaysia region, we further extended the time series to the years 1981-2017 using

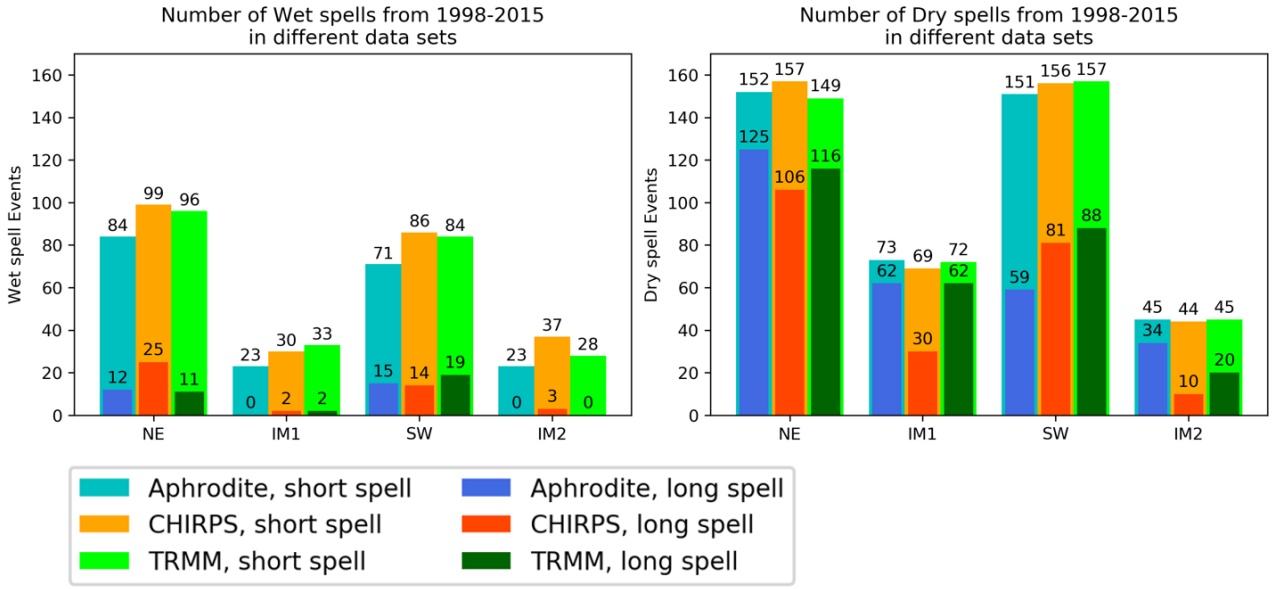

Figure 5: Bar charts showing the number of short and long wet spells (left) and the number of short and long dry spells (right) from 1998 to 2015, for individual seasons and using different precipitation products computed for the D2 domain.

the CHIRPS data set (Figure 6). Anomalies were calculated from the new climatology spanning 1981-2017, and dry and wet spells, both short and long, were classified similarly using the same method employed for determining dry and wet spells, as described in the "Data and Methods" section.

Between 1981 – 2017, we noted that there were more short wet spells (48, 18, 51 and 19) in La-Niña phase

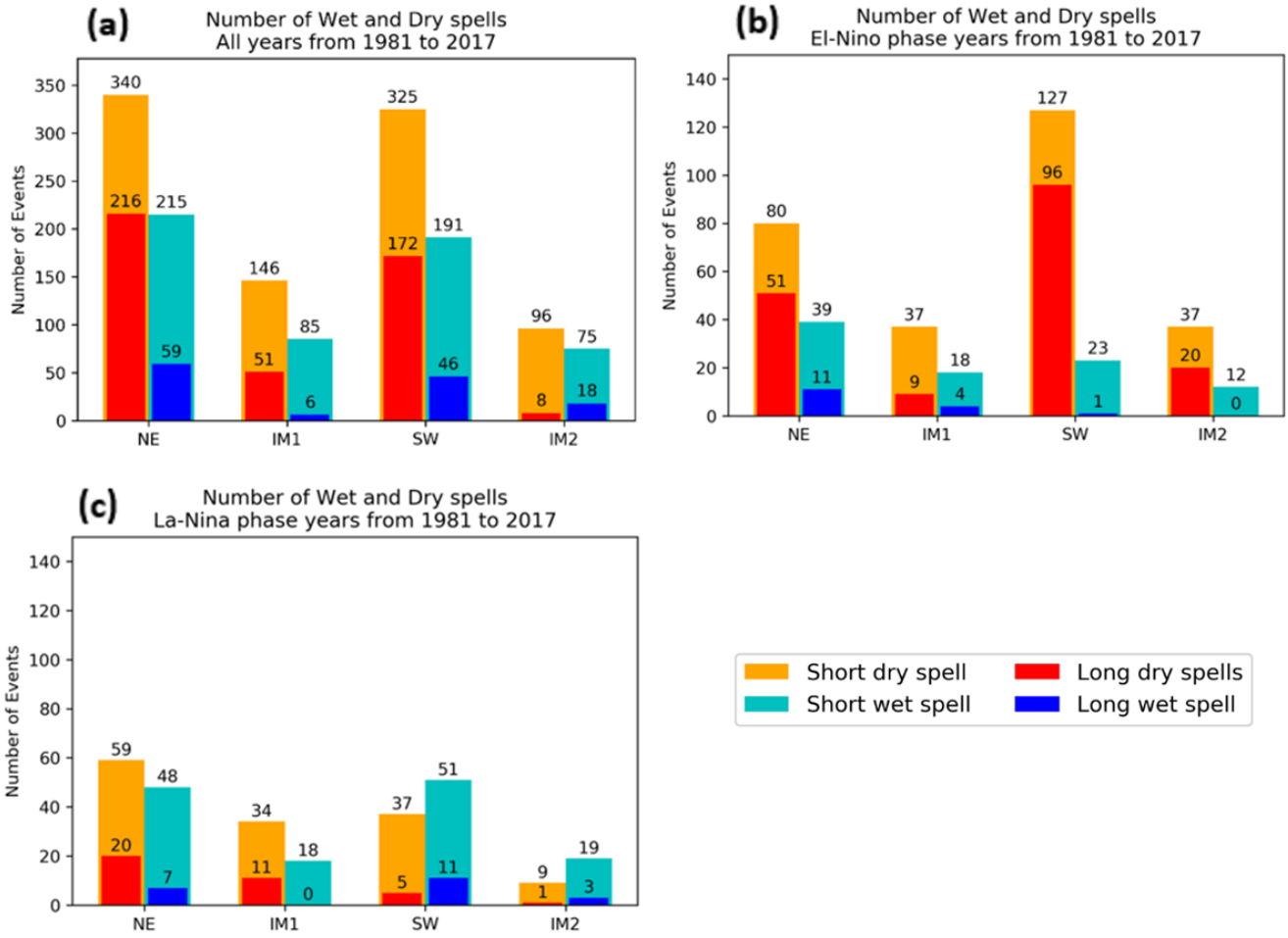

Figure 6: Number of wet and dry spells from 1981 to 2017 calculated using CHIRPS, for (a) all years, (b) El-Niño phase years only, (c) La-Niña phase years only computed for the D2 domain.

years (figure 6c) compared to El-Niño phase years (39, 18, 23 and 12) (figure 6b) across all seasons, except for IM1 which showed an equal number of short wet spells for both El-Niño and La-Niña years. However, there were more long wet spells in El-Niño years for the NE monsoon (11) and IM1 (4), while there were more long wet spells in La-Niña years for the SW monsoon (11) and IM2 (3).

There were more dry spells during El-Niño years than in La-Niña years, whether short or long. The number of dry spells, both short (127) and long (96), was highest during El-Niño years in the SW monsoon season. There were more wet spells, whether short (51) or long (11) than dry spells (37, 5) during La-Niña years in the SW monsoon. During the NE monsoon there were more dry spells (59, 20) compared to wet spells (48, 7) during La-Niña years.

Both IM1 and IM2 showed fewer wet spells (18, 0 and 19, 3), whether short or long, as well as fewer dry spells (34, 11 and 9, 1) during La-Niña years compared to the SW and NE monsoon seasons. The wet spells reduced from 191, 46 for all years to 23, 1 during El-Niño years in the SW monsoon. Similarly, dry spells in the Inter monsoon, particularly for IM2, reduced from 96, 8 for all years to 9, 1 during La-Niña years. Therefore, the SW monsoon and Inter monsoon seasons were the most affected by the El-Niño and La-Niña phases.

Apart from computing the number of long and short wet and dry spells for the four seasons (NE, IM1, SW and IM2), we also analysed their year-to-year variability for four seasons for the two different periods (1998-2015 using all 3 datasets, 1981-2017 using CHIRPS only). The following is a summary of the results for 1998 – 2015: Although it seems that the number of long dry spells was increasing during the NE monsoon (p=0.22) and the SW monsoon (p=0.79), this increase was statistically insignificant. The number of long wet spells in the NE monsoon appeared to be increasing (p=0.081). The number of dry spells appeared to have been decreasing during IM1 (p = 0.04) and IM2 (p=0.014), from the mean of the three datasets (APHRODITE, CHIRPS and TRMM; Figure 7). However, as the trend was not obvious, we also cannot reliably conclude from these 18 years of data that there has been an increase in the number of short dry spell events; a longer data period must be used to determine the trend in the spells over the years. Except for the long dry spells in the NE and SW monsoons in 2015 and the long dry spells during the inter-monsoons in 1998 and 1999, there is little variability in the number of dry and wet spells among the three datasets (Aphrodite, CHIRPS and TRMM). This low variability in terms of dry or wet spells identified each year suggests that the three data sets are reliable when compared with one another and may be a good estimate of the precipitation data over the Indonesia-Malaysia region.

The results from similar analyses using the CHIRPS precipitation data over the longer period of 37 years from 1981- 2017 are presented in Figure 8, where we observed the following: 1)The trend of wet spells and dry spells (both long and short) seemed to be less obvious; 2) The dry (wet) spell peaks coincided with El-Niño (La-Niña) phase; 3) There was a slight decreasing trend in short dry spells and increasing trend in short wet spells during all seasons except IM1; 4) There appeared to be a slight increasing trend in short wet spells (p=0.017) and long wet spells (p=0.0091). We also discerned statistically significant trends in the number of spells in IM1 and IM2, but this trend was much smaller than the increase in trend in short wet spells during the NE monsoon. Although we see slight increasing or decreasing trends, these are not very obvious and the data period used is also very short. Therefore, a longer data period and more rigorous significant testing is needed to identify if there are any trends in wet/dry spells during different seasons.

Spell intensity was calculated by taking the accumulated anomaly rainfall during a spell, divided by the number of days in the spell. Although there were more dry than wet spell events, the intensities of dry and wet spells are not equal. Wet spells in the SW monsoon were more intense than dry spells, with a higher absolute mean standard anomaly per spell, for both short and long spells. We noticed an increasing trend in the intensity of long wet spells (p = 0.11) and a decreasing trend in long dry spells (p = 0.09) from 1981 to 2017 in the NE monsoon. This trend also appears in the SW monsoon, where there may be an increasing trend in the intensity of long wet spells (p = 0.13) and a decreasing trend in the intensity of long dry spells (p=0.19).

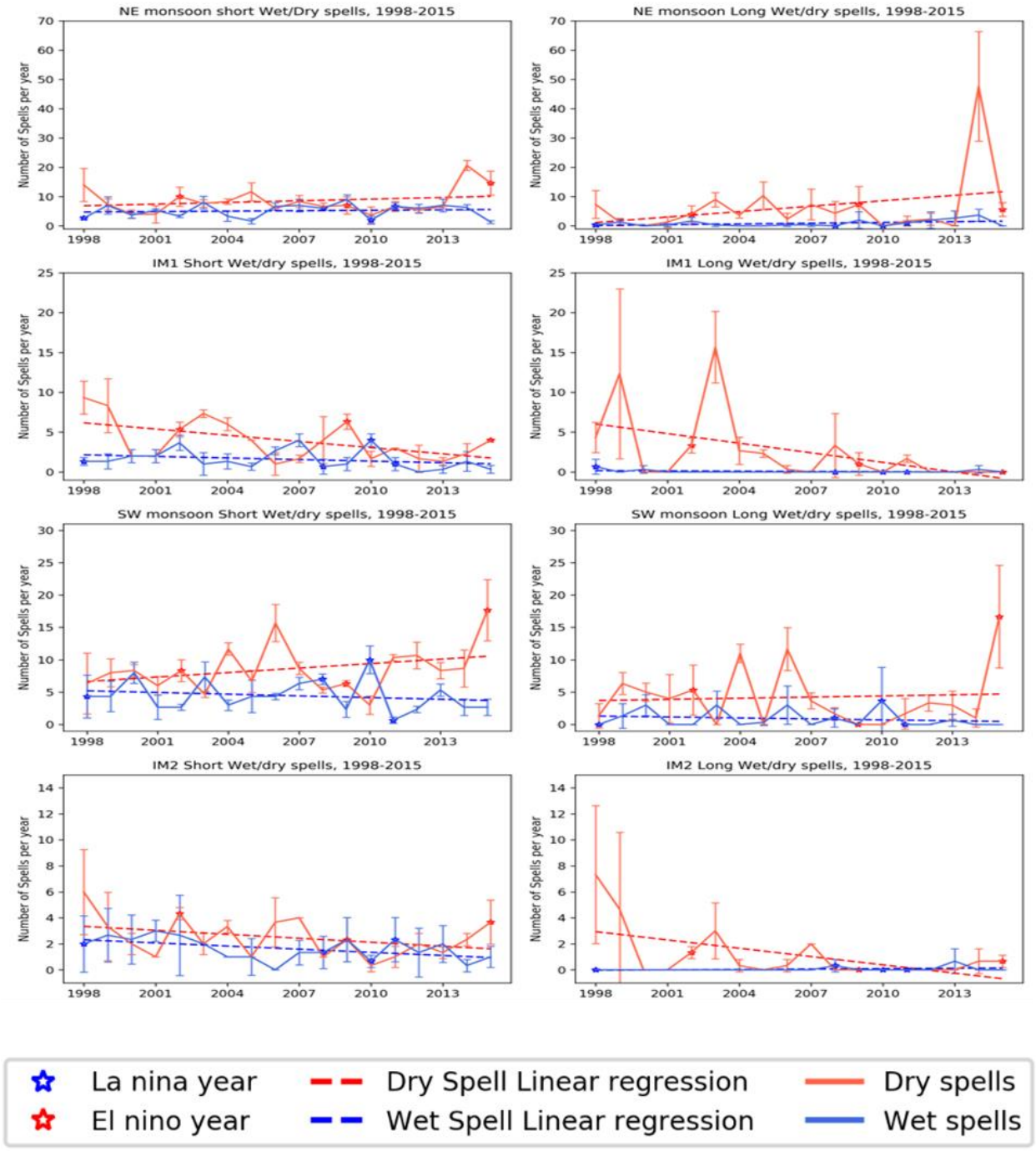

Figure 7: Temporal distribution of number of short (left) and long (right) wet and dry spell events per season from 1998-2015 over the Indonesia-Malaysia region (D2). The dashed lines are the linear regression for the dry spells (red) and wet spells (blue). Each data point represents the average of the APHRODITE, CHIRPS and TRMM. The bars denote the lower and upper ranges from the three different datasets.

There appears to be a decreasing trend in the intensity of long wet spells in IM1 (p=0.93) and IM2 (p=0.31) and an increasing trend in the intensity of long dry spells in both IM1 (p = 0.79) and IM2 (p = 0.70) (Figure 9), which are statistically insignificant. In fact, the trends shown in each season do not appear to be significant. Due to the smaller number of long wet and dry spells from 1981 to 2017, more data needs to be analysed to determine the long-term trend in wet and dry spells. By classifying the spells into La-Niña, El-Niño and Neutral years only, we observed a statistically significant decreasing trend in the intensity of short dry spells over the 8 La-Niña years (p = 0.07). This was the only statistically significant trend obtained over all the monsoon seasons.

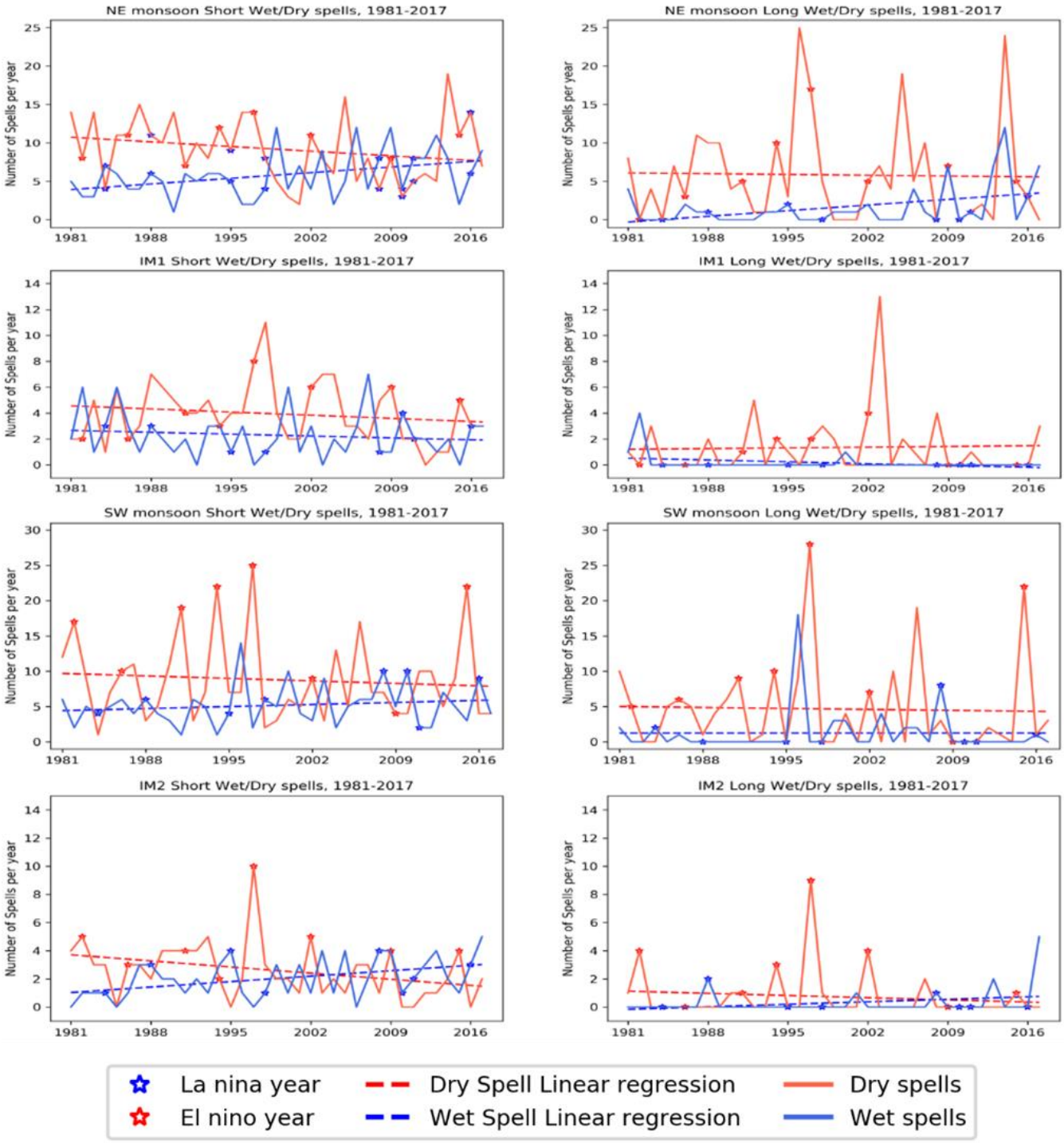

Figure 8: Temporal distribution of the number of short (left) and long (right) wet and dry spell events per season from 1981-2017 computed for the D2 domain. Red stars denote El Niño Years, blue stars denote La Niña Years. Dashed red lines denote dry spell linear regression and dashed blue lines denote wet spell linear regression.

For the wet and dry spells in the Indonesian-Malaysian region from 1981 to 2017 using CHIRPS data, dry spells were greater in number during El-Niño years compared to La-Niña years for all seasons, whether short or long. Short wet spells were greater in number during La-Niña years compared to El-Niño years for all seasons except for the SW monsoon where short wet spells were equal in number in El-Niño and La-Niña years. Long wet spells in the neutral phase of the ENSO showed the strongest absolute precipitation anomaly, across all four monsoon seasons (Figure 10).

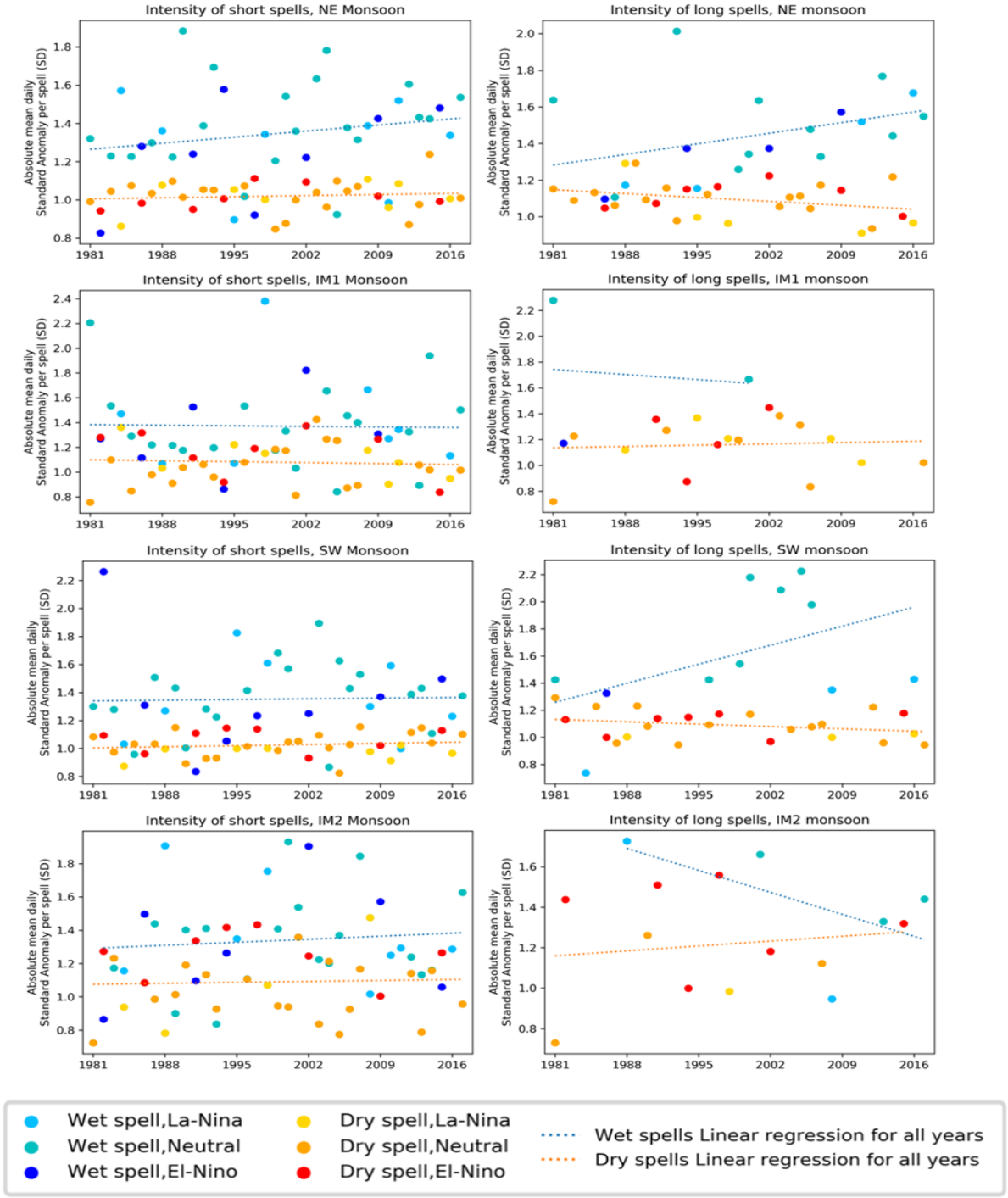

Figure 9: Temporal distribution of mean daily wet and dry spell intensity per season from 1981-2017 computed for the D2 domain. Spell intensities are plotted for each year, and they are classified into El-Niño, La-Niña and Neutral years represented by different coloured dots.

4 CONCLUSION

This study used multiple datasets over the maritime continent and compared the datasets for seasonal and daily means and variability. Although the precipitation from these three products (APHRODITE, CHIRPS and TRMM) have similar large scale patterns within the Indonesia-Malaysia region, they do differ in daily mean and standard deviation for each season.

The study also brought out the differences among the datasets in capturing the precipitation variabilities and the active (wet) and break (dry) cycles within each season. Wet and dry spells during the different monsoon seasons in the Indonesia-Malaysia region have been characterised using three precipitation products, APHRODITE, CHIRPS and TRMM.

We compared the representation of each dataset for short and long dry and wet spells for each season and

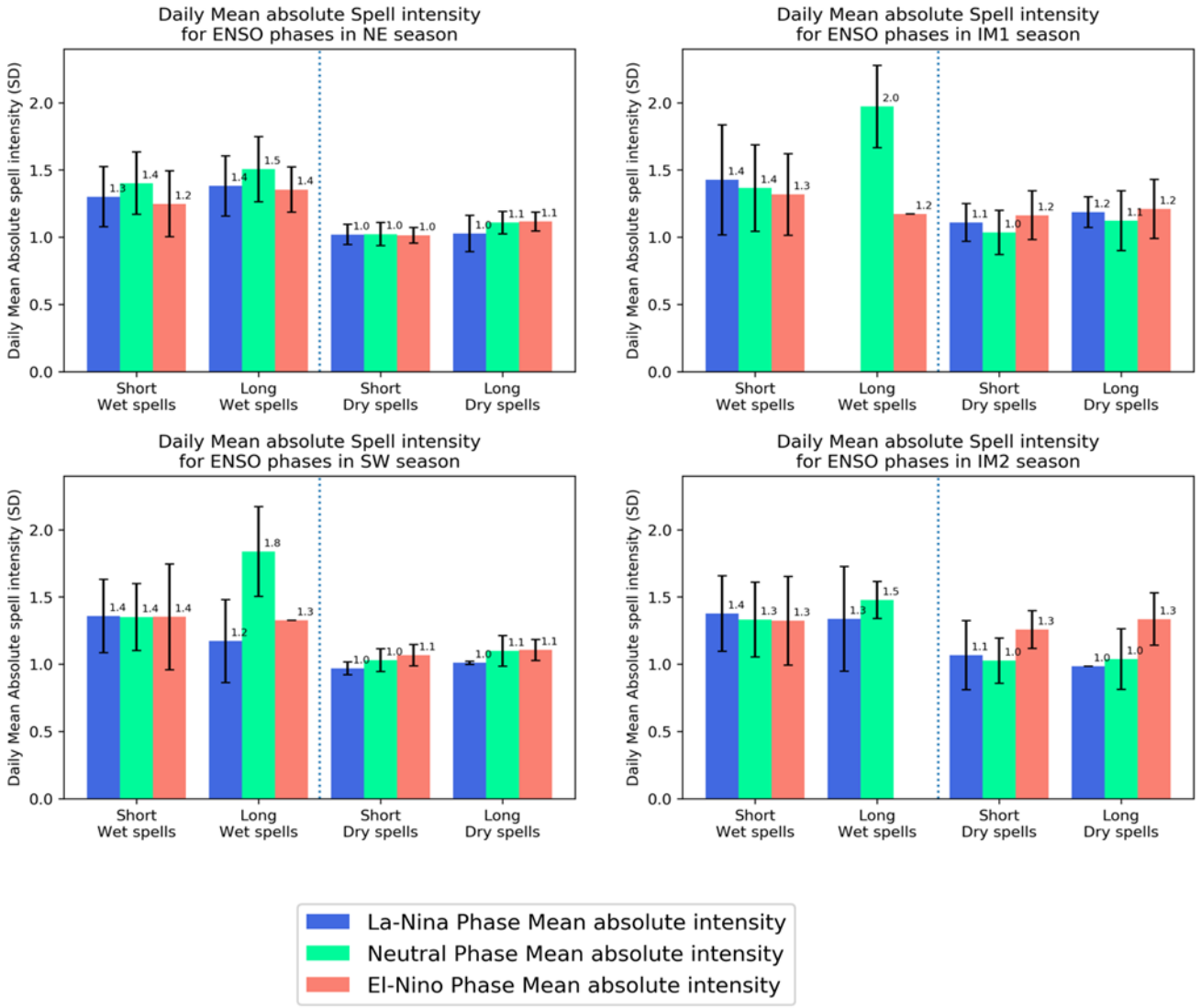

Figure 10: Bar charts showing mean wet and dry spell intensity for different ENSO phases in different monsoon seasons from 1981-2017 computed for the D2 domain.

their inter-annual variability for the available data period over the Indonesia-Malaysia region. We also compared the characteristics of short and long dry and wet spells during ENSO years. We found that during El Niño years, the dry spells were more pronounced during the SW monsoon season compared to other monsoon seasons. Although there were generally fewer wet spell events than dry spell events over the Indonesia-Malaysia region during 1981-2017, wet spells appeared to be more intense than dry spells.

ENSO had differing impacts on the number and intensity of wet spells and dry spells for each monsoon season. The ratio of wet spells to dry spells differed most during the SW monsoon and IM2 during El-Niño years compared to La-Niña years. The mean daily intensity of wet and dry spells was also affected by the ENSO phases.

There were limitations in this study. The active and break spells were identified using a threshold of +/- 0.5 daily standard deviation for wet and dry cycles, and the spells were defined as having a duration of 3 days for short spells and greater than or equal to 7 days for long spells. We performed sensitivity tests to the thresholds before fixing these thresholds, as we know that the assumption of normal distribution of rainfall introduces uncertainty in defining the active and break phases. The method is simple but effective in characterising the active break cycle over this region.

More research needs to be done on the trends in the frequency and number of wet and dry spells in recent years, and further studies could focus on the effect of ENSO on the monsoon seasons using the onset and demise dates of ENSO phases or the developing and decay phases of ENSO, rather than using the ENSO phase for the entire year as used in this study.

5 References

Cheong, W.K., Timbal, B., Golding, N., Sirabaha, S., Kwan, K.F., Cinco, T.A., Archevarahuprok, B., Vo, V.H., Gunawan, D. and Han, S. (2018), 'Observed and modelled temperature and precipitation extremes over Southeast Asia from 1972 to 2010', *International Journal of Climatology*, 38:3013-3027 https://doi.org/10.1002/joc.5479

Fong, M. (2012), The Weather and Climate of Singapore. Meteorological Service Singapore. ISBN 9789810713409

Funk, C., Peterson, P., Landsfeld, M., Pedreros, D., Verdin, J., Shukla, S., Husak, G., Rowland, J., Harrison, L., Hoell A. and Michaelsen, J. (2015), 'The climate hazards infrared precipitation with stations—a new environmental record for monitoring extremes', *Scientific Data* volume 2, Article number: 150066. DOI: 10.1038/sdata.2015.66

Hassim, M. E. E. and Timbal, B. (2019), 'Observed rainfall trends over Singapore and the Maritime Continent from the perspective of regional large scale weather regimes', *Journal of Applied Meteorology and Climatology* 58: 365-384. DOI: https://doi.org/10.1175/JAMC-D-18-0136.1

He, Y.J. (2018), 'Exploration of the monsoon seasons over Singapore: "Determining the local onset and retreat dates of the monsoon and inter-monsoon periods"', CCRS Internship report. 2018.

Huffman, G.J., Adler, R.F., Bolvin, D.T., Gu, G., Nelkin, E.J., Bowman, K.P., Hong, Y., Stocker, E.F. and Wolff, D.B. (2007), 'The TRMM Multisatellite Precipitation Analysis (TMPA): Quasi-Global, Multiyear, Combined-Sensor Precipitation Estimates at Fine Scales', *Journal of Hydrometeorology*, 8:38–55. DOI:10.1175/JHM560.1

Prasanna, V. (2016), 'Heavy precipitation characteristics over India during the summer monsoon season using rain gauge, satellite and reanalysis products', *Nat Hazards*, Volume 83, Issue 1, pp 253–292. DOI 10.1007/s11069-016-2315-z

Turkington, T., Timbal, B. and Rahmat, R. (2018), 'The impact of global warming on sea surface temperature based El Niño–Southern Oscillation monitoring indices', *International Journal of Climatology*, 1–12. https://doi.org/10.1002/joc.5864

Yatagai, A., Kamiguchi, K., Arakawa, O., Hamada, A., Yasutomi, N. and Kitoh, A. (2012), 'APHRODITE: Constructing a Long-term Daily Gridded Precipitation Dataset for Asia based on a Dense Network of Rain Gauges', *Bulletin of the American Meteorological Society*: 1401 - 1415, DOI:10.1175/BAMS-D-11-00122.1

GLOSSARY*

APHRODITE-2 (Asian Precipitation - Highly-Resolved Observational Data Integration Towards Evaluation -2): a set of long-term (1951 onward) continental-scale daily products that is based on a dense network of rain-gauge data for Asia including the Himalayas, South and Southeast Asia and mountainous areas in the Middle East.

BASE: A series of nested chemistry transport models for air quality simulation.

CAPE (most unstable): Most Unstable Convective Available Potential Energy (MUCAPE, J/kg) represents the total amount of potential energy available to the most unstable parcel of air found within the lowest 300hPa of the atmosphere while being lifted to its level of free convection (LFC). The CAPE calculation uses the virtual temperature correction.

Climate Hazards Group InfraRed Precipitation V2.0 (CHIRPS): a high-resolution gridded precipitation dataset which is available at a daily time scale, with a spatial resolution of 0.05° x 0.05°. It is built upon a global 0.05° precipitation climatology and incorporates gridded precipitation estimates from cold-cloud estimates, station data and satellite measurements from 1981-present.

CMAQ (Community Multi-scale Air Quality): an active open-source development project of the U.S. Environmental Protection Agency that consists of a suite of programs for conducting air quality model simulations. CMAQ combines current knowledge in atmospheric science and air quality modeling, multi-processor computing techniques, and an open-source framework to deliver fast, technically sound estimates of ozone, particulates, toxics and acid deposition.

Cross Totals (CT): The CT index is commonly used as a severe weather indicator and is based on temperature and moisture data. $CT = Td_{850} - T_{500}$

Dry Slot (surface – 7000ft): A low-level dry air layer (RH <= 50%) from the surface to ~2km Above Ground Level (AGL) may suppress or delay convective activity. The presence of a low-level dry slot is quite rare in tropical regions and typically occurs in synoptic scale.

Jefferson Index: The Jefferson index (JI) is a stability index, tested and used in maritime areas. $JI = 1.6 \times WBPT_{850} - T_{500} - 0.5 \times dew\text{-}point\_depression_{700} - 8$, where: WBPT is wet-bulb potential temperature.

K-Index (KI): The KI is a function of 850hPa, 700hPa and 500hPa temperature and moisture information (Hart & Korotky, 91). $KI = T_{850} + Td_{850} - T_{700} + Td_{700} - T_{500}$

Lifted index (LI): The LI is calculated as the difference between the observed temperature at 500hPa and the temperature of an air parcel lifted to 500hPa from low-level Lifted Condensation Level (LCL). The low-level LCL is found by using the mean moisture content in the lower 1km. The more unstable the environment, the more negative the LI.

Mean-mixing Ratio (surface to 950hPa): This mean-mixing ratio (MMR) is defined as the ratio of the mass of water vapour to the mass of dry air (in g/kg) averaged from the surface level to 500m AGL.

MEGAN (Model of Emissions of Gases and Aerosols from Nature) version 2: a modelling system for estimating the net emission of gases and aerosols from terrestrial ecosystems into the atmosphere, used here for biogenic emissions estimation.

Mid-level Dry Slot x Mid-level Wind Speed: A deep mid-level dry air incursion (RH <= 50%) when combined with strong mid-level winds from ~2km to ~6.5km AGL may suppress deep convection totally due to dry air entrainment and shearing of growing clouds.

NOFIRE: A set of air quality simulation without biomass burning emissions.

Precipitable Water: This is the total precipitable water of the entire column of air represented by the plotted sounding and represents a vertical integration of mean mixing ratios.

Relative Humidity (surface to 750hPa): Relative humidity (Mean RH, in %) is a measure of the actual amount of water vapour in the air compared to the total amount of vapour that can exist in the air at its current temperature and pressure. This parameter is averaged from the surface level to 2.5km AGL.2

Shear Speed (surface to 700hPa): The shear speed (surface to 700hPa) represents the vector difference between the winds (in knots) at the surface level and 3km AGL.

Steering-level wind speed (900hPa to 700hPa): The steering-level wind speed (Storm speed) is the average-layer wind speed (in knots) from 1km to 3km above ground level (AGL). This 1-3km layer typically represents the bulk movement of thunderstorms in the tropics.

Tropical Rainfall Measuring Mission (TRMM): a precipitation product designed to measure precipitation in the tropics. TRMM 3B42 with a spatial resolution of 0.25° x 0.25° provides a 3-hourly accumulated precipitation product, measured using satellite sensors.

Vorticity Generation Parameter (VGP): The VGP is the rate at which horizontal vorticity is converted to vertical vorticity through tilting.

Wet-Bulb Zero (WBZ) Height: WBZ height is the height (in feet) where the wet-bulb profile transitions from a positive to a negative temperature. It is commonly used as one of many factors in estimating hail size and severe weather potential.

World Meteorological Organisation (WMO): An agency under the United Nations for meteorology (both weather and climate), as well as operational hydrological services.

700-500 Lapse Rate: The 700-500 lapse rate (°C/km) is the temperature difference between 700hPa (3km AGL) and 500hPa (6km AGL) and then divided by a thickness of 3km. For this paper, a 700-500 lapse rate of < -6 °C/km corresponds to instability in the mid-level atmosphere while values > -5 °C/km indicate a stable mid-level atmosphere.

*Information related to heavy rain predictors (Kang and Boh, MSS Research Letters 6 #2) is mainly obtained from 'RAOB User Guide & Technical Manual' and Northern Territory Regional Office's severe thunderstorm directive.

Website: ccrs.weather.gov.sg

Address: 36 Kim Chuan Road, Singapore 537054